DEVELOPMENT OF A COMBINED -RITZ METHOD FOR MODELING 3D ACOUSTICS IN CANDU FUEL SUB-CHANNELS

by

David Andres Villero

B.Sc., Physics and Astrophysics,

University of Toronto, 2013

A thesis

presented to Ryerson University in partial fulfillment of the

requirements for the degree of Master of Applied Science

in the Program of Mechanical Engineering

Toronto, Ontario, Canada, 2015

AUTHOR'S DECLARATION FOR ELECTRONIC SUBMISSION OF A THESIS

I hereby declare that I am the sole author of this thesis. This is a true copy of the thesis, including any required final revisions, as accepted by my examiners.

I authorize Ryerson University to lend this thesis to other institutions or individuals for the purpose of scholarly research.

I further authorize Ryerson University to reproduce this thesis by photocopying or by other means, in total or in part, at the request of other institutions or individuals for the purpose of scholarly research.

I understand that my thesis may be made electronically available to the public.

DEVELOPMENT OF A COMBINED -RITZ METHOD FOR MODELING 3D ACOUSTICS IN CANDU FUEL SUB-CHANNELS

Master of Applied Science 2015

David Villero

Graduate Program of Mechanical Engineering

Ryerson University

Abstract

A combined finite element-Ritz method is developed to effectively model the 3D low-frequency acoustics in CANDU fuel sub-channels. The complex acoustic behavior of CANDU fuel sub-channels in the cross section is captured using the six-node isoparametric triangular elements; and the acoustic wave propagation in the axial direction is modeled using the polynomials of order n. The Lagrange equations are utilized to formulate the system equations of motion. The acoustic system considered in this study consists of pipe-like medium (water) with rigid and smooth walls. At the inlet of the fuel channel acoustic system, an acoustic pressure wave is prescribed to simulate the pulsation induced by the main feeder pumps. At the outlet, the acoustic system is assumed to interact with a reacting and absorbing material with prescribed acoustic impedance. The method was tested for several scenarios of interest. Numerical results obtained are in excellent agreement with the analytical and ANSYS solutions.

ACKNOWLEDGEMENTS

Table of Contents

LIST OF TABLES

LIST OF FIGURES

NOMENCLATURE

$[B]$	Strain-displacement matrix
c	Speed of sound (m/s)
$[\widetilde{C}]_e$	Element impedance damping matrix
$[\tilde{C}_{zz}]_e$	Z component element impedance damping matrix
$[\tilde{C}]$	Global damping matrix
d_a	Impedance damping coefficient
$\{\overline{F}\}$	Force vector
J^e	Element Jacobian matrix
k_a	Impedance stiffness coefficient
k	Wave number
$[K_e]$	Element stiffness matrix
$[K_{xx}]_e$	X component element stiffness matrix
$[K_{yy}]_e$	Y component element stiffness matrix
$[K_{zz}]_e$	Z component element stiffness matrix
$[K_{xy}]_e$	XY component element stiffness matrix
$[K_{xz}]_e$	XZ component element stiffness matrix
$[K_{yz}]_e$	YZ component element stiffness matrix
$[\tilde{K}]_e$	Element impedance stiffness matrix
$[K]$	Global stiffness matrix
$[\tilde{K}_{zz}]_e$	Z component element impedance stiffness matrix

$[K]$	Generalized global stiffness matrix
l	Length of domain (m)
$[M]$	Global mass matrix
$[M_e]$	Element mass matrix
$[M]$	Global mass matrix
n	Order of polynomial
$[N_1]$	Isoparametric shape function
$[N_2]$	Ritz shape function
P_0	Initial piston pressure
p	Acoustic pressure (Pa)
$\hat{p}_L$	Complex acoustic pressure (Pa)
$\{p_e\}$	Impedance element pressure
$\{Q_{AI}\}$	Generalized force vector
$\{Q_{zs}\}$	Moving boundary force vector
r	Domain radius
t	Time (s)
T	Kinetic energy
$\{\bar{u}\}$	Global acoustic displacement vector
$\{\bar{u}_e\}$	Element acoustic displacement vector
$\{\bar{u}_e\}$	X component element acoustic displacement vector
$\bar{u}_i$	X component nodal acoustic displacement coefficient

$\dot{u}_n$	Acoustic velocity normal to surface
$\bar{v}_i$	Y component nodal acoustic displacement coefficient
$\{\bar{v}_e\}$	Y component element acoustic displacement vector
$\hat{v}_L$	Complex acoustic velocity
V	Potential energy
V_0	Initial piston velocity
$\{\bar{w}_e\}$	Z component element acoustic displacement vector
$\bar{w}_i$	Z component nodal acoustic displacement coefficient
x, y, z	Cartesian coordinates
Z_n	Acoustic impedance normal to surface
Z_r	Real acoustic impedance
Z_i	Imaginary acoustic impedance

Greek symbols

β, γ	Newmark parameters
κ_s	Bulk modulus (Pa)
φ	Normal angle
η	Non-dimensional coordinate, $\frac{z}{l}$
ζ, ξ	Natural coordinates of six-node 2D finite element
ρ	Density ($Kg.m^3$)
ω	Excitation frequency (rads/sec)

ω_b	Burst frequency
ϵ	Strain component

Abbreviations

CANDU	Canada Deuterium Uranium
	Finite element
LES	Large Eddy Simulation

CHAPTER 1   INTRODUCTION

This chapter is divided into three sections that introduce the background of the research, the research objective and the proposed methodology. Section 1.1 presents a description of a CANDU reactor along with the observed phenomenon of bundle vibration and the possible driving mechanisms, including acoustic induced excitation, which is the main focus of this study. Section 1.2 highlights the main objective of this study and introduces the assumptions made for the development of the acoustic model. Section 1.3 presents a combination of finite element with Ritz method as the proposed scheme to simulate acoustic waves in a CANDU fuel channel.

1.1   Background

In a CANDU reactor, fission reactions are used to heat pressurized heavy water in a primary cooling loop. The heated heavy water runs through arrays of pipes for steam generation. This secondary cooling loop powers a steam turbine that is attached to an electric generator. The exhaust steam is condensed and re-used as feed water to the steam generator (Rouben, 2005).

The CANDU-6 reactor core consists of approximately 400 fuel channels. Each fuel channel is a pressurized tube that contains a string of 12 or 13 fuel bundles and heavy water operating at approximately 10 MPa and 300°C, with a mass flow rate of 15-20 $kg \cdot s^{-1}$. A shield plug that is designed to hold all bundles against the hydraulic drag supports the downstream fuel bundle. In the CANDU-6 model, each bundle is designed to have 37 fuel elements of which 18 are located in the outer ring, 12 in the middle ring and 6 in the inner ring. This leaves one at the center.

Under normal reactor operations, the bundles have been known to show noticeable vibration caused by fluid flow, acoustic resonance or fluid-acoustic structure interaction. Given the design of the bundles, they can show small-scale motions inside the tube such as rolling, sliding and bending vibration with respect to the designed equilibrium position. This induces friction and impact between the bundles and the pressure pipe which, over a long period of time, appears to be damaging the pressure pipe and the fuel bundle bearing pads. The bundle motion can cause wear and material-loss of the pressure pipe, also known as fretting, along with endplate cracking.

As a practical example for bundle vibration due to acoustic resonance, it has been reported that the Darlington and Bruce reactors have shown the presence of endplate cracking at the outlet bundles. It was also demonstrated that pressure pulsations originated from the water pump were acoustically amplified in certain fuel channels. Especially, a pulsation frequency of 150 Hz coincided with the resonant frequency of the inner seven fuel elements of the 37-element bundle. These acoustic pulsations not only induced small rolling motion but they also cause the bundles to vibrate in the axial direction. Axial vibration at the resonant frequency led to endplate cracking (Wenhui & Manzer, 1991).

1.1.1 Fuel Bundle Vibration Phenomenon

The vibration phenomenon of the fuel bundle can be a result of a particular mechanism or a combination of multiple mechanisms. One of these mechanisms, and the main focus of this study, is acoustic induced excitation. The acoustic pressure pulsations originated

from the pumps can be a source of low frequency acoustic excitation. Solid structures are not seriously affected by high frequencies but rather low frequency pressure waves, since low frequencies generally cause the structure to respond with a large displacement. Also, if the frequency of this acoustic pressure wave matches or is close to one of the natural frequencies of the structure, acoustic resonance may be observed. In the literature concerning the vibration phenomena of the fuel bundle, many studies have presented computer and numerical models to examine the vibration of the fuel bundle in which acoustic excitation is not included (Zhang and Yu, 2008; Bhattacharya, Yu & Kawall, 2012; Bhattacharya, Yu & Kawall, 2013). To generate an accurate approximation of behavior of the fuel bundle, it is necessary to account for all the sources of vibration. Therefore, there is a need for the implementation of an accurate and efficient acoustic model that is able to capture small fluctuation within sub-channels. In addition to acoustic induced excitation, other mechanisms that may be responsible for the fuel bundle vibration phenomena are: fluid-elastic instability, vortex shedding and turbulence-induced excitation.

1.1.2 *Finite Element Acoustics Literature Review*

In the literature, Gladwell and others (1966) originally formulated the development of finite element analysis for acoustic problems. A variational method was used to derive the appropriate finite element form of the acoustic wave equation (see Appendix A) Gladwell also discussed the formulation of structural-acoustic interaction, the impedance boundary condition, and the Sommerld radiation conditions. This work was successful and forms the basis for most subsequent finite element work in acoustics. Gladwell also formulated the acoustic problem in terms of acoustic velocity. The applicable governing

equation remains the wave equation with the acoustic velocity as the variable, hence a vector equation. As a result, for three-dimensional problems, the equations of motion for the velocity formulation of the problem will be three times as large as for the corresponding pressure formulation. For this reason, Gladwell concluded that the pressure formulation was more efficient. However, some investigations continue to use a velocity formulation because the fluid dynamic problems cannot be simplified to the pressure wave equation (Astley and Eversman, 1971). In other studies, rewriting the velocity formulation to a displacement formulation showed that dealing with non-conservative forces and interfacial conditions can be easily implemented if Lagrange multipliers are used (Yu and Kawall, 2013).

In the field of computational acoustics, early pioneers like Gladwell and Zimmerman (1966) and Young (1994) presented models where they used sub-parametric[1] elements for their investigations. For these types of elements, the acoustic variables used at the nodes are the pressure and the pressure gradients. These models are able to capture the propagation of acoustic waves in complex domains very well and show smaller transient solutions. However, the models often become large and consequently result in programs that are expensive to run. Craggs showed that, unlike dynamic and structural problems, the detail provided by the pressure gradients was, in most cases, not necessary and that typical acoustic problems could be run with a single acoustic pressure variable at each node. However, this model requires very fine meshed domains in order to acquire the desired accuracy (1972). Every one of these studies uses a full implementation of finite

---

[1] In the finite element method a sub – parametric element is an element that uses more field nodes than geometrical nodes.

elements, which, in many cases, raises problems of computational time and is limited to studying the propagation of acoustic waves in simple domains.

1.2   Objectives and Assumptions

The objective of this research is to develop an accurate acoustic model to study acoustic wave propagation in a three-dimensional domain. The model should capture the behavior of acoustic pressure in localized regions. The model is meant to study the acoustic induced excitation phenomenon and, therefore, the acoustic response of a fluid medium inside a CANDU fuel channel in order to determine the acoustic excitations on individual fuel elements or the entire bundle. The mathematical formulation for the acoustic model is implemented into a Python/C++ code and a Fortran code so as to suit specific applications, such as acoustic – structure interaction studies of elongated structures and domains.

In this study, the following assumptions are made: 1) It is assumed that flow does not affect or induces acoustic waves in the system, hence the fluid flow is negligible; 2) To avoid energy losses in the system, it is assumed that the pipe walls are smooth, rigid and adiabatic; 3) Since the acoustic source is assumed to not be generated by fluid turbulence, viscous forces are assumed to be small and therefore the fluid is inviscid. These assumptions are applied to every system model in this study. Essentially, these assumptions cause the acoustic waves to behave linearly and facilitate the validation of the results with the appropriate analytical solution for the system or by comparison against numerical results from an FE software such as ANSYS. Further, the fuel channel

system is simplified by studying the system when all bundles are aligned so that there are no sub-channel discontinuities from one bundle to the next. Hence the system takes the form of one long bundle.

1.3   FE-Ritz Method

Many engineering acoustic problems are modeled and solved using a finite element-based commercial software package that offers a sufficient accuracy with an acceptable computational time. However, when an acoustic system gets large and requires a very fine mesh to capture local and detailed phenomena, the traditional FE analysis becomes computationally expensive.
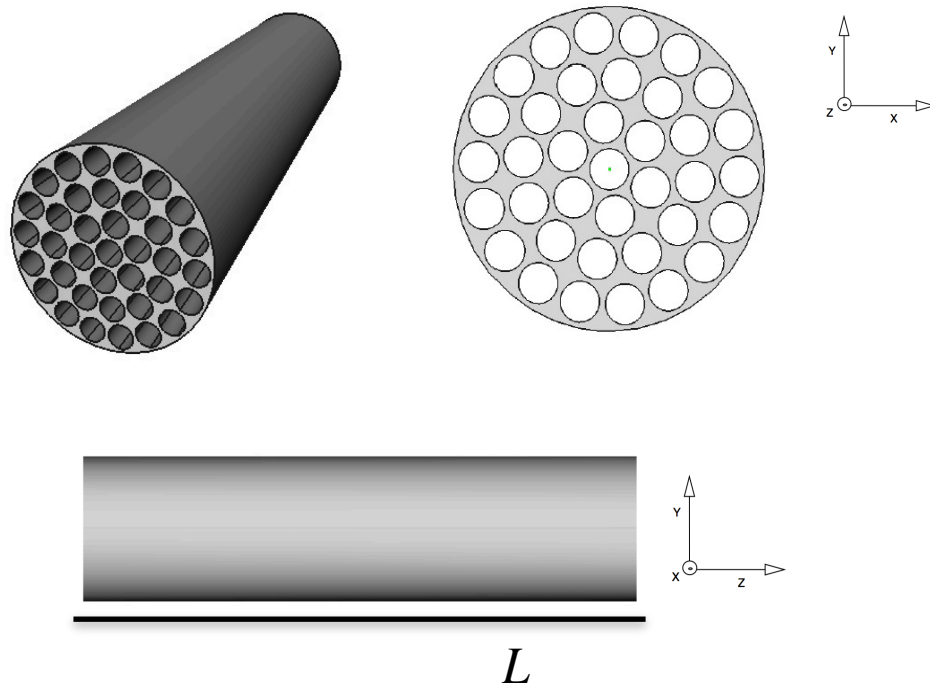
Figure 1.1: Geometrical characteristics of fuel Channel.

In this study, a combined finite element - Ritz method is proposed for handling low frequency acoustics in a CANDU fuel channel with complex cross sectional sub-channel geometry. The idea is to model the acoustic behavior of fluid particles within the bundle's coherent sub-channel system at a cross-section with a conventional 2D FE method and capture any acoustic fluctuations along the axial direction by means of a global polynomial expansion, or Ritz method (Hjelmstad, 2005). The combination of a 2D method with a 1D approximation is used to approximate the propagation of acoustic pulsating waves in a three-dimensional domain. By employing this method, one is able to reduce the number of degrees of freedom of the desired problem, and thus the computational time, without jeopardizing the accuracy of the solution.

For the mathematical formulation, a displacement-based method is used to examine the propagation of three-dimensional acoustic waves through a fluid medium. Compared to the classical pressure-based approach used by Craggs (1976), Hackett (1976), and Gladwell (1996), a displacement-based formulation as used by Yu and Kawall (2013) allows the derivation of the equations of motion by Hamilton's variation principle, which facilitates the implementation of non-classical boundary conditions and interface conditions between distinct domains and media. Since the acoustic pressure is a derived quantity, it can be obtained at the post-processing stage of the FE analysis.

In finite element method, the elements used to discretize a particular domain are divided into 3 categories: iso-parametric, sub-parametric and super-parametric[2] elements. Iso-parametric elements are those in which the shape functions are the same for both geometric and field variables, (Fish & Belytschko, 2007) (Onate, 2009). To approximate the acoustic displacement and account for deformation for a fluid particle, the six-node iso-parametric triangular elements are used to discretize the cross-sectional plane. On the other hand, the variations of the acoustic displacement in the direction normal to the discretized plane are handled using a polynomial interpolation. This method uses the polynomial expansion as a way of extruding the 2D mesh so that the three-dimensional domain is divided into prism elements. As an illustrative example, Figure 1.2 shows a graphical representation of fluid-filled region for a 37-rod CANDU fuel channel in which acoustic waves propagate.

---

[2] In the finite element method, a super–parametric element is an element that uses more geometrical nodes than field nodes.
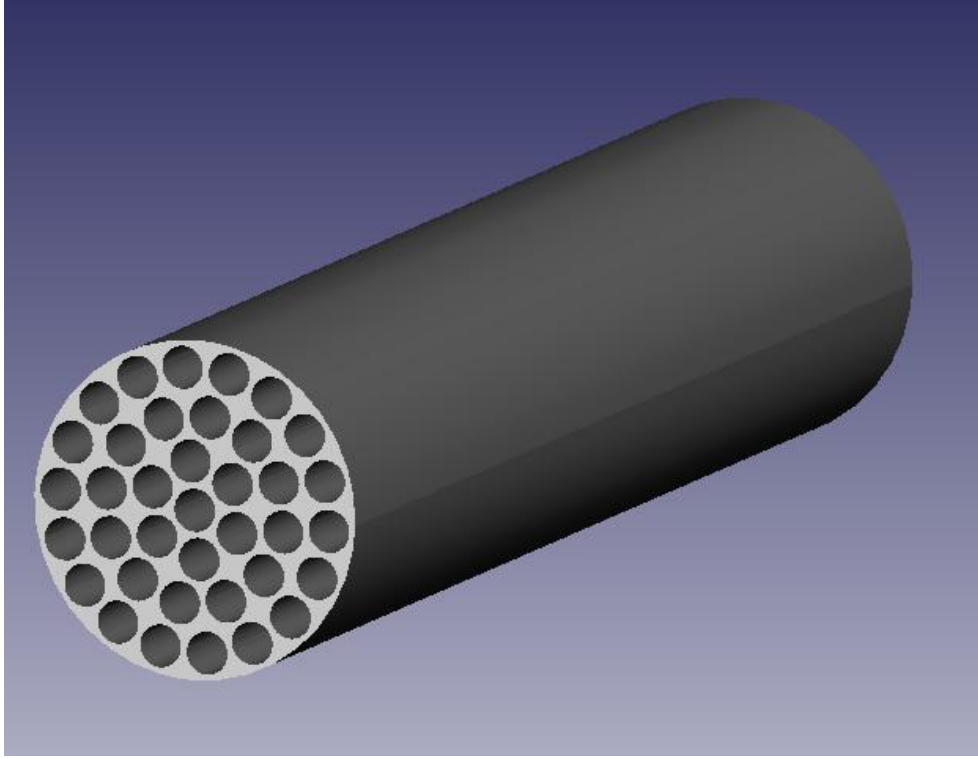
Figure 1.2: Fluid domain in a fuel channel.

Ideally, the domain depicted in Figure 1.2 is discretized using FE-Ritz elements. The cross sectional surface is first meshed and is then extruded by linearly combining it with a global polynomial expansion of nth order.
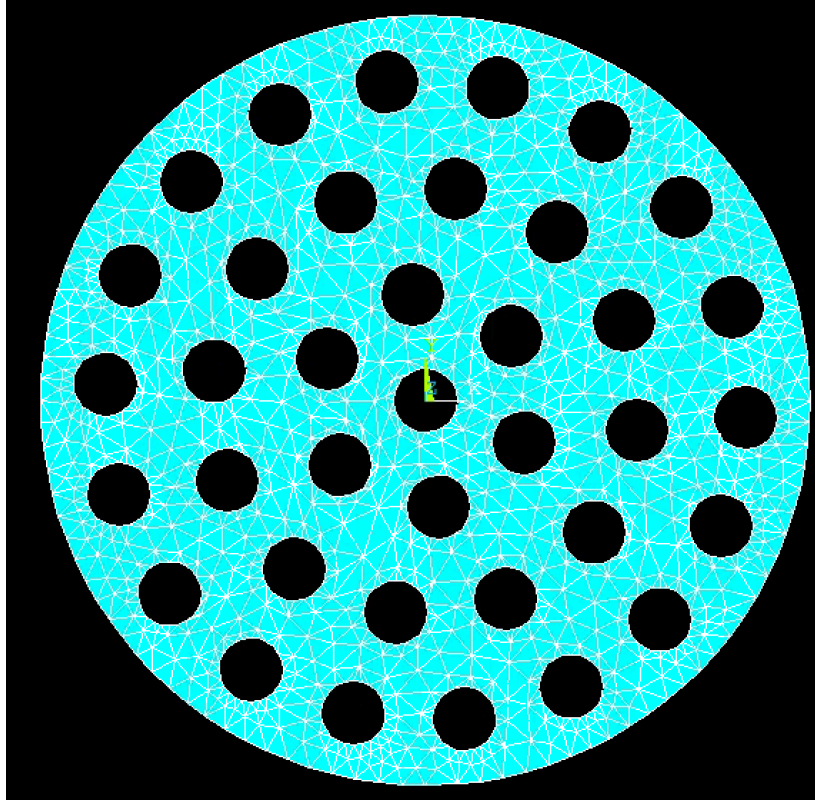
Figure 1.3: Bundle Cross-section meshed using 6 – node triangular elements.

1.4   Chapter Summary

This chapter provides a brief description of the CANDU nuclear reactor, its bundle vibration problem and the potential causes. Further, it presents the phenomenon of acoustic induced excitation as the main topic of this study along with a literature review on computational acoustics. This chapter highlights the main objective as the development of an acoustic model to study acoustic induced vibration in a CANDU fuel channel. The assumptions made for the implementation of the acoustic model are also introduced. Lastly, a description of the proposed FE-Ritz method and the logic behind is presented in the last section.

CHAPTER 2   3D ACOUSTIC SIMULATION

This chapter presents the mathematical formulation for the combined finite element - Ritz method. Section 2.1 introduces the derivation of the component mass and stiffness matrices for one FE – Ritz method; Section 2.2 explains the implementation of boundary conditions, generalized forces and the derivation of equations of motion; Section 2.3 illustrates the post–processing procedures to obtain nodal pressure from nodal displacement quantities. In addition to the mathematical derivation, this chapter also presents a brief discussion of Newmark's method (Zienkiewicz, Taylor and Fox, 2013).

2.1 Finite Element Formulation of Acoustic System

The acoustic model is constructed to simulate the propagation of acoustic waves within coherent sub-channels in a fuel-channel system. An approximation is introduced by expressing the displacement components in terms of linear combinations of shape functions, which are locally defined within small subdomains ('finite elements') and interpolated with a polynomial of nth order. In this way, the original problem of determining the acoustic displacement components at any position in the fluid domain may be approximately transformed into a problem of determining the acoustic displacement coefficients at some discrete positions in the fluid domain.

The acoustic system component is modeled using six-node isoparametric three-dimensional prism elements, as shown in Figure 2.1. This element is constructed by a combination of a 2D element and a polynomial expansion.

11
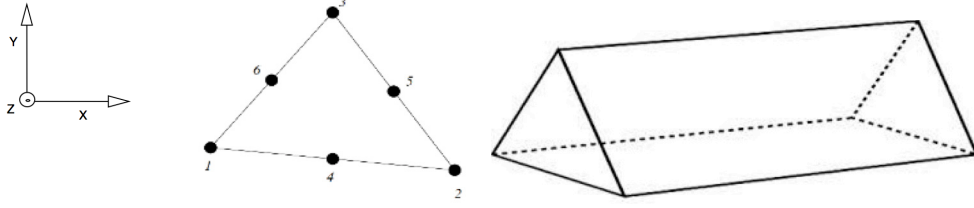
Figure 2.1: FE-Ritz three-dimensional prism element.

Within each element, the acoustic displacement field varies with local natural coordinates, ξ, η and ζ,

$$u_{xe} = [N_1(\xi,\eta)] \begin{bmatrix} [N_2(\zeta)] & \dots & 0 \\ \vdots & \ddots & 0 \\ 0 & 0 & [N_2(\zeta)] \end{bmatrix} \left\{ \begin{matrix} \left\{ \begin{matrix} \bar{u}_{x0} \\ \vdots \\ \bar{u}_{xn} \end{matrix} \right\}_1 \\ \left\{ \begin{matrix} \bar{u}_{x0} \\ \vdots \\ \bar{u}_{xn} \end{matrix} \right\}_2 \\ \vdots \\ \left\{ \begin{matrix} \bar{u}_{x0} \\ \vdots \\ \bar{u}_{xn} \end{matrix} \right\}_6 \end{matrix} \right\} \tag{2.1.1}$$

$$[N_1(\xi,\eta)]^T = \begin{bmatrix} \xi(2\xi - 1) \\ \eta(2\eta - 1) \\ (1 - \xi - \eta)(2(1 - \xi - \eta) - 1) \\ 4(1 - \xi - \eta)\eta \\ 4\eta(1 - \xi - \eta) \\ 4(1 - \xi - \eta)\xi \end{bmatrix} \tag{2.1.2}$$

is the shape function for a general six-node isoparametric triangle (Zienkiewicz, Taylor and Fox, 2013).

$$[N_2(\zeta)] = [1 \; \zeta \; \zeta^2 \; ... \; \zeta^n] \tag{2.1.2}$$

is the shape function for the linear combination of polynomials, where ζ is the normalized

coordinate $\frac{z}{L}$; and $\begin{Bmatrix} \bar{u}_{x0} \\ \vdots \\ \bar{u}_{xn} \end{Bmatrix}$ are the displacement coefficient vectors for each node

(Hjelmstad, 2005).

The displacement along the y and z directions, $\bar{u}_{ye}$ and $\bar{u}_{ze}$, respectively, resembles the

same form as that of u_{xe}. Also, note that the field variable chosen to formulate the

equations of motion for the acoustic system is the acoustic displacement as opposed to

the acoustic pressure, which can eventually be derived from the acoustic displacement.

The kinetic and potential energy can be written as:

$$T = \frac{1}{2} \iiint_{\Omega_e} \rho \, (\dot{\boldsymbol{u}})^2 dV = \sum_{e=1}^{N_e} \frac{1}{2} \{\dot{\bar{\boldsymbol{u}}}_e\}^T [M_e]\{\dot{\bar{\boldsymbol{u}}}_e\} \tag{2.1.3}$$

$$V = \frac{1}{2} \iiint_{\Omega_e} \rho c^2 \, (\nabla \cdot \boldsymbol{u})^2 dV = \sum_{e=1}^{N_e} \frac{1}{2} \{\bar{\boldsymbol{u}}_e\}^T [K_e]\{\bar{\boldsymbol{u}}_e\} \tag{2.1.4}$$

where $\{\bar{\boldsymbol{u}}_e\} = \begin{Bmatrix} \bar{u}_x \\ \bar{u}_y \\ \bar{u}_z \end{Bmatrix}_e$, the element mass $[M_e]$, and stiffness matrix $[K_e]$ are calculated as:

13

$$[M_e] = \begin{bmatrix} [M]_e & 0 & 0 \\ 0 & [M]_e & 0 \\ 0 & 0 & [M]_e \end{bmatrix} \tag{2.1.5}$$

$$[M]_e = \iiint_{\Omega_e} \rho [N_2(\xi,\eta)]^T [N_1(\zeta)]^T [N_1(\zeta)][N_2(\xi,\eta)]|J|\, d\xi\, d\eta\, d\zeta \tag{2.1.6}$$

and

$$[K]_e = \begin{bmatrix} [K_{xx}]_e & [K_{xy}]_e & [K_{xz}]_e \\ [K_{yx}]_e & [K_{yy}]_e & [K_{yz}]_e \\ [K_{zx}]_e & [K_{zy}]_e & [K_{zz}]_e \end{bmatrix} \tag{2.1.7}$$

for which each of the stiffness components can be computed individually as:

$$[K_{xx}]_e = \int_0^1 \kappa_s [\bar{N}_2(\zeta)]^T \left(\int_{A_e} [N'_{1,x}]^T [N'_{1,x}]|J|\, d\xi\, d\eta\, d\gamma \right) [\bar{N}_2(\zeta)] l d\zeta \tag{2.1.8}$$

$$[K_{yy}]_e = \int_0^1 \kappa_s [\bar{N}_2(\zeta)]^T \left(\int_{A_e} [N'_{1,y}]^T [N'_{1,y}]|J|\, d\xi\, d\eta\, d\gamma \right) [\bar{N}_2(\zeta)] l d\zeta \tag{2.1.9}$$

$$[K_{zz}]_e = \int_0^1 \kappa_s [\bar{N}'_{2,z}(\zeta)]^T \left(\int_{A_e} [N_1]^T [N_1]|J|\, d\xi\, d\eta\, d\gamma \right) [\bar{N}'_{2,z}(\zeta)] l d\zeta \tag{2.1.10}$$

And since $[K]_e$ is symmetric

$$[K_{xy}]_e = [K_{yx}]_e = \int_0^1 \kappa_s [\bar{N}_2(\zeta)]^T \left(\int_{A_e} [N'_{1,x}]^T [N'_{1,y}]|J|\, d\xi\, d\eta\, d\gamma \right) [\bar{N}_2(\zeta)] l d\zeta \tag{2.1.11}$$

$$[K_{xz}]_e = [K_{zx}]_e = \int_0^1 \kappa_s [\bar{N}'_{2,z}(\zeta)]^T \left(\int_{A_e} [N'_{1,x}]^T [N_1] |J| \, d\xi \, d\eta \, d\gamma \right) [\bar{N}'_{2,z}(\zeta)] l d\zeta \qquad (2.1.12)$$

$$[K_{zy}]_e = [K_{yz}]_e = \int_0^1 \kappa_s [\bar{N}_2(\zeta)]^T \left(\int_{A_e} [N'_{1,y}]^T [N_1] |J| \, d\xi \, d\eta \, d\gamma \right) [\bar{N}'_{2,z}(\zeta)] l d\zeta \qquad (2.1.13)$$

Once the formulation for one element component vector is determined, one can relate the element nodal displacements to the global component vector through a transformation matrix $[T_{e \to g}]$, as follows

$$\{\bar{u}_e\} = [T_{e \to g}] \{\bar{u}\} \qquad (2.1.14)$$

One can further use this transformation to obtain the kinetic and potential energies in terms of the global nodal displacement as:

$$T = \frac{1}{2} \{\dot{\bar{u}}\}^T [M] \{\dot{\bar{u}}\} \qquad (2.1.15)$$

$$V = \frac{1}{2} \{\bar{u}\}^T [K] \{\bar{u}\} \qquad (2.1.16)$$

where the component mass and stiffness matrix are:

$$[M] = \sum_{e=1}^{N_e} [T_{e \to g}]^T [M_e] [T_{e \to g}]$$

15

$$[K] = \sum_{e=1}^{N_e} [T_{e \to g}]^T [K_e][T_{e \to g}]$$

The following Lagrange equations are used to obtain the system equations of motion

$$\frac{d}{dt}\left(\frac{\partial L}{\partial \{\dot{\boldsymbol{u}}\}^T}\right) - \frac{\partial L}{\partial \{\overline{\boldsymbol{u}}\}^T} = 0 \tag{2.1.17}$$

where $L = T - V$. Substituting the expressions for the kinetic and potential energy into Eq. (2.1.18) and in the absence of external forces, we arrive at

$$[M]\{\ddot{\overline{\boldsymbol{u}}}\} + [K]\{\overline{\boldsymbol{u}}\} = 0 \tag{2.1.18}$$

In finite element, the boundary conditions of the corresponding system are usually implemented in a separate matrix or into the stiffness matrix. In many cases, certain boundary conditions will reduce the degrees of freedom while in many others the degrees of freedom can increase. This depends on what the boundary conditions are and how they are implemented.

2.2 Acoustic Boundary Conditions and Equations of Waves

Taking into account that the main focus of the proposed FE-Ritz method is to study the propagation of acoustic waves in duct-like domains, it is important to mention the physical characteristics of the internal surfaces. In acoustic studies, it is often desired to describe boundary conditions in terms of acoustic impedance (Bernhard, 1982). Acoustic impedance is defined as the ratio of the acoustic pressure to the normal acoustic velocity at the boundary

$$p = Z_n \dot{u}_n \qquad (2.2.1)$$

where Z_n is the acoustic impedance, p is the acoustic pressure and $\dot{u}_n$ is the acoustic velocity normal to the boundary.

The relation between the acoustic velocity and pressure can be written in terms of pressure by using the governing equations (Appendix A)

$$\frac{\partial p}{\partial n} = -\frac{\rho}{Z_n}\frac{\partial p}{\partial t} \qquad (2.2.2)$$

When studying acoustics, there are two idealized boundary conditions (Bernhard, 1982): a perfective reflective wall and a completely absorbent or anechoic boundary. In the literature, it is common to find a description of reflective boundaries in terms of pressure,

$$\frac{\partial p}{\partial n} = 0 \qquad (2.2.3)$$

From Eq. (2.2.2) this means that $Z_n = \infty$. For a completely absorbent boundary, the wave propagates as though no boundary were present and thus the pressure at the boundary is

$$p = \rho c \dot{u}_n \qquad (2.2.4)$$

Hence, from Eq. (2.2.1) the acoustic impedance, $Z_n = \rho c$ (Bernhard, 1982).

In many cases, the walls are not perfectly rigid and the system is confined to a finite space, making the boundaries both absorbent and reflective. The complex specified acoustic impedance is defined as:

$$\frac{\hat{p}_L}{\rho c \hat{v}_L} = Z_r + iZ_i \qquad (2.2.5)$$

where, $\hat{v}_L$ is the complex velocity at the boundary, Z_r is the real part of the acoustic impedance, Z_i is the imaginary part of the acoustic impedance, ρ is the density of the medium and c is the speed of the wave in the medium.

2.2.1 *Prescribed Acoustic Impedance of Absorbent and Reactive Walls*

When acoustic impedance is imposed at one of the system's boundaries (i.e. the outlet of the pressure pipe), the boundary will dynamically affect the system as it responds to incoming acoustic energy. In a sense, this boundary absorbs and reflects some of the incoming acoustic wave, which generates a pressure at all points on the boundary. This pressure can be interpreted as a generalized force $\{Q_{AI}\}$, generalized forces are defined by the boundary's behavior. Yu and Kawall (2013) defined the pressure generated by the specified acoustic impedance through the following relation:

$$\{p\} = k_a\{u_z\} + d_a\{\ddot{u}_z\}$$
(2.2.6)

where the stiffness k_a and damping d_a coefficients correspond to the imaginary and real parts of the acoustic impendence. If the incoming acoustic pulsation wave has a frequency ω, the stiffness and damping coefficients are defined as:

$$k_a = Z_i\rho c\omega$$
(2.2.7)

$$d_a = Z_r\rho c$$
(2.2.8)

18

The pressure generated only depends on the axial acoustic displacement u_z. Therefore, the generalized force vector is take the form:

$$\{Q_{AI}\} = -\sum_{e=1}^{N_e} \iint_{\Gamma} \{\overline{u}_z\}^T [N_2]^T [N_1]^T|_{z=L} (k_a [N_1]|_{z=L} [N_2]\{\overline{u}_z\} + d_a [N_1]|_{z=L}[N_2]\{\dot{\overline{u}}_z\}) dA \tag{2.2.9}$$

The generalized force vector can be written as

$$\{Q_{AI}\} = -\sum_{e=1}^{N_e} \left(\{\overline{u}_z\}^T [\tilde{K}_{zz}] \{\overline{u}_z\} + \{\overline{u}_z\}[\tilde{C}_{zz}] \{\dot{\overline{u}}\} \right) \tag{2.2.10}$$

This force vector is the sum of the non-conservative damping and stiffness forces related to a damping and a stiffness matrix respectively, which are defined as:

$$[\tilde{C}]_e = \begin{bmatrix} 0 & 0 & 0 \\ 0 & 0 & 0 \\ 0 & 0 & [\tilde{C}_{zz}]_e \end{bmatrix} \tag{2.2.11}$$

where

$$[\tilde{C}_{zz}]_e = \iint_{\Gamma} d_a [N_2]^T [N_1]^T|_{z=L} [N_1]|_{z=L} [N_2]|J| d\xi \, d\eta \tag{2.2.12}$$

and

$$[\tilde{K}]_e = \begin{bmatrix} 0 & 0 & 0 \\ 0 & 0 & 0 \\ 0 & 0 & \tilde{K}_{zz\,e} \end{bmatrix} \tag{2.2.13}$$

where

19

$$[\widetilde{K}_{zz}]_e = \iint_\Gamma k_a [N_2]^T [N_1]^T |_{z=L} [N_1]|_{z=L} [N_2] |J| d\xi \, d\eta$$

(2.2.14)

Since the generalized force only acts with respect to axial variations, the other components are zero. One can then add the stiffness contribution of the reacting boundary to the component stiffness matrix [K]. The global generalized forces can write as follows

$$\{Q_p\} = -[\widetilde{K}]\{\overline{u}\} - [\widetilde{C}]\{\dot{\overline{u}}\}$$

(2.2.15)

for which the Global component non-conservative stiffness and damping matrices are

$$[\widetilde{K}] = \sum_{e=1}^{N_e} [T_{e \to g}]^T [\widetilde{K}]_e [T_{e \to g}]$$

(2.2.16)

$$[\widetilde{C}] = \sum_{e=1}^{N_e} [T_{e \to g}]^T [\widetilde{C}]_e [T_{e \to g}]$$

(2.2.17)

2.2.2   Second Order Differential Equations of Waves

The equations of waves in the acoustic system may be obtained from solving the following Lagrange equations:

$$\frac{d}{dt}\left(\frac{\partial L}{\partial \{\dot{\overline{u}}\}^T}\right) - \frac{\partial L}{\partial \{\overline{u}\}^T} = \{Q\}$$

(2.2.18)

where $\{\overline{u}\}$ is the nodal acoustic displacement vector and $\{Q\}$ are the generalized forces. Substituting Equations (2.1.15), (2.1.16) and (2.2.15) into Equation (2.2.18) yields the following second order partial differential equations for the unconstrained system

20

$$[M]\{\ddot{\overline{u}}\} + [K]\{\overline{u}\} = -[\widetilde{K}]\{\overline{u}\} - [\widetilde{C}]\{\dot{\overline{u}}\} \qquad (2.2.19)$$

Naturally, Eq. (2.2.19) is the discretized form of the general wave equation in three dimensions where $[\widetilde{K}]$ and $[\widetilde{C}]$ are the generalized force matrices that appear due to the prescribed acoustic impedance at the outlet of the system. It is worth mentioning that Eq. (2.1.9) to Eq. (2.1.13) as well as Eq. (2.2.19) can also be obtained from the weak formulation of the general wave equation (Appendix A) by a Galerkin method[3] (Zienkiewicz, Taylor and Fox, 2013).

---

[3] Gelerkin methods are a class of variation methods used to obtain the weak formulation of an equation.

2.3 Post-Processing for Acoustic FE-Ritz Model

After solving the system, Eq. (2.2.19) the nodal coefficients solution is obtained as

$$\{\bar{u}\} = \left\{ \begin{array}{c} \left\{ \begin{array}{c} \bar{u}_{x0} \\ \vdots \\ \bar{u}_{xn} \end{array} \right\}_1 \\ \left\{ \begin{array}{c} \bar{u}_{y0} \\ \vdots \\ \bar{u}_{yn} \end{array} \right\}_1 \\ \left\{ \begin{array}{c} \bar{u}_{z0} \\ \vdots \\ \bar{u}_{zn} \end{array} \right\}_1 \\ \vdots \\ \left\{ \begin{array}{c} \bar{u}_{x0} \\ \vdots \\ \bar{u}_{xn} \end{array} \right\}_6 \\ \left\{ \begin{array}{c} \bar{u}_{y0} \\ \vdots \\ \bar{u}_{yn} \end{array} \right\}_6 \\ \left\{ \begin{array}{c} \bar{u}_{z0} \\ \vdots \\ \bar{u}_{zn} \end{array} \right\}_6 \end{array} \right\} \tag{2.3.1}$$

Further, one can use these nodal coefficients to compute the pressure using the pressure-displacement relations:

$$p = -\rho c^2 \left(\varepsilon_{xx} + \varepsilon_{yy} + \varepsilon_{zz} \right) \tag{2.3.2}$$

which is related to the acoustic displacement by

$$p = -\rho c^2 \left(\frac{\partial u}{\partial x} + \frac{\partial v}{\partial y} + \frac{\partial w}{\partial z} \right) \tag{2.3.3}$$

22

where the divergence of the displacement defines the volumetric strain. For a finite element, the strain-displacement matrix (Zienkiewicz, Taylor and Fox, 2013) can write as:

$$
[B] = \begin{bmatrix}
\dfrac{\partial N_{1i}}{\partial x} N_2(z) & 0 & 0 \\[2mm]
0 & \dfrac{\partial N_{1i}}{\partial y} N_2(z) & 0 \\[2mm]
0 & 0 & N_{1i} \dfrac{\partial N_2}{\partial z}(z) \\[2mm]
\dfrac{\partial N_{1i}}{\partial y} N_2(z) & \dfrac{\partial N_{1i}}{\partial x} N_2(z) & 0 \\[2mm]
0 & N_{1i} \dfrac{\partial N_2}{\partial z}(z) & \dfrac{\partial N_{1i}}{\partial y} N_2(z) \\[2mm]
N_{1i} \dfrac{\partial N_2}{\partial z}(z) & 0 & \dfrac{\partial N_{1i}}{\partial x} N_2(z)
\end{bmatrix} \quad \cdots
\tag{2.3.4}
$$

where

$$
\frac{\partial N_2}{\partial z} = \begin{bmatrix}
0 \\
\dfrac{1}{L} \\[2mm]
\dfrac{2}{L}\left(\dfrac{z}{L}\right) \\[2mm]
\vdots \\
\dfrac{n}{L}\left(\dfrac{z}{L}\right)^{n-1}
\end{bmatrix}
\tag{2.3.5}
$$

and the partial derivatives of N_1 are calculated as

$$
\begin{Bmatrix}
\dfrac{\partial N_{1i}}{\partial x} \\[2mm]
\dfrac{\partial N_{1i}}{\partial y}
\end{Bmatrix}
= \frac{1}{|J^e|}
\begin{bmatrix}
\dfrac{\partial y}{\partial \eta} & -\dfrac{\partial y}{\partial \xi} \\[2mm]
-\dfrac{\partial x}{\partial \eta} & \dfrac{\partial x}{\partial \xi}
\end{bmatrix}
\begin{Bmatrix}
\dfrac{\partial N_{1i}}{\partial \xi} \\[2mm]
\dfrac{\partial N_{1i}}{\partial \eta}
\end{Bmatrix}
\tag{2.3.6}
$$

23

where $|J^e|$ is the determinant of the Jacobian matrix[4] which is calculated as

$$J^e = \sum_{i=1}^{n=6} \begin{bmatrix} \dfrac{\partial N_{1_i}}{\partial \xi} x_i & \dfrac{\partial N_{1_i}}{\partial \xi} y_i \\[3mm] \dfrac{\partial N_{1_i}}{\partial \eta} x_i & \dfrac{\partial N_{1_i}}{\partial \eta} y_i \end{bmatrix} \qquad (2.3.7)$$

By multiplying the strain-displacement matrix by the nodal coefficients vector, one obtains the strain components:

$$\begin{Bmatrix} \varepsilon_{xx} \\ \varepsilon_{yy} \\ \varepsilon_{zz} \\ \varepsilon_{xy} \\ \varepsilon_{yz} \\ \varepsilon_{xz} \end{Bmatrix} = \begin{bmatrix} \dfrac{\partial N_{1_i}}{\partial x} N_2(z) & 0 & 0 \\[3mm] 0 & \dfrac{\partial N_{1_i}}{\partial y} N_2(z) & 0 \\[3mm] 0 & 0 & N_{1_i} \dfrac{\partial N_2}{\partial z}(z) \\[3mm] \dfrac{\partial N_{1_i}}{\partial y} N_2(z) & \dfrac{\partial N_{1_i}}{\partial x} N_2(z) & 0 \\[3mm] 0 & N_{1_i} \dfrac{\partial N_2}{\partial z}(z) & \dfrac{\partial N_{1_i}}{\partial y} N_2(z) \\[3mm] N_{1_i} \dfrac{\partial N_2}{\partial z}(z) & 0 & \dfrac{\partial N_{1_i}}{\partial x} N_2(z) \end{bmatrix} \cdots \begin{Bmatrix} \begin{Bmatrix} \bar{u}_{x0} \\ \vdots \\ \bar{u}_{xn} \end{Bmatrix}_1 \\ \begin{Bmatrix} \bar{u}_{y0} \\ \vdots \\ \bar{u}_{yn} \end{Bmatrix}_1 \\ \begin{Bmatrix} \bar{u}_{z0} \\ \vdots \\ \bar{u}_{zn} \end{Bmatrix}_1 \\ \vdots \\ \begin{Bmatrix} \bar{u}_{x0} \\ \vdots \\ \bar{u}_{xn} \end{Bmatrix}_6 \\ \begin{Bmatrix} \bar{u}_{y0} \\ \vdots \\ \bar{u}_{yn} \end{Bmatrix}_6 \\ \begin{Bmatrix} \bar{u}_{z0} \\ \vdots \\ \bar{u}_{zn} \end{Bmatrix}_6 \end{Bmatrix} \qquad (2.3.8)$$

The strain is a function of the triangular coordinates ξ and η. Hence, the pressure is calculated at a specific location.

---

[4] The Jacobian matrix defines a linear map $R^n \rightarrow R^m$, and in finite element it relates the natural coordinate space n, to the global coordinate space m.

In acoustic studies, pressure is a better way of interpreting the results, which is why the post-processing is done once the time integration is finished. In the present formulation, the time integration should yield displacement, velocity and acceleration and the accuracy and convergence rate of the results usually depend on the order of the method used. For this study, the method used is Newmark's method due to its capacity to yield accurate solutions for dynamic problems.

2.4 Time Integration: Newmark's Method

In order to solve Eq. (2.2.19), one is required to discretize it with respect to time so that it can be integrated. For dynamic problems, it is recommended to use implicit integration methods such as Newmark's method (Zienkiewicz, Taylor and Fox, 2013) because of its unconditional stability and accuracy.

In Newmark's method, the ability of obtaining stable and accurate solutions depends on the correct choice of the parameters β, and γ. It is worth highlighting that the method can be made unstable for $\gamma < 1/2$ and unconditionally stable for $2\beta \geq \gamma \geq 1/2$. Additionally, these parameters can also be handled to introduce artificial damping ($\gamma > 1/2$), which may reduce the accuracy.

To discretize the equation, one must first write the displacement, velocity and acceleration at time $t + \Delta t$:

$$\{\overline{u}\}_{t+\Delta t} = \{\overline{u}\}_t + \Delta t\{\dot{\overline{u}}\}_t + \left[(1-\beta)\{\ddot{\overline{u}}\}_t + \beta\{\ddot{\overline{u}}\}_{t+\Delta t}\right]\Delta t^2 \qquad (2.4.1)$$

$$\{\dot{\overline{u}}\}_{t+\Delta t} = \{\dot{\overline{u}}\}_t + \left[(1-\gamma)\{\ddot{\overline{u}}\}_t + \gamma\{\ddot{\overline{u}}\}_{t+\Delta t}\right]\Delta t \qquad (2.4.2)$$

$$\{\ddot{\overline{u}}\}_{t+\Delta t} = \frac{1}{\Delta t^2\beta}\left[-\{\overline{u}\}_t - \Delta t\{\dot{\overline{u}}\}_t - \Delta t^2\left(\frac{1}{2}-\beta\right)\{\ddot{\overline{u}}\}_t + \{\overline{u}\}_{t+\Delta t}\right] \qquad (2.4.3)$$

The recurrence formula for Eq. (2.2.19), subjected to an external force load $\{\overline{F}\}$ at time $t+\Delta t$ can be written as follows:

$$[M]\{\ddot{\overline{u}}\}_{t+\Delta t} + [\tilde{C}]\{\dot{\overline{u}}\}_{t+\Delta t} + [K]\{\overline{u}\}_{t+\Delta t} = \{\overline{F}(t+\Delta t\} \qquad (2.4.4)$$

where $[K] = [K] + [\tilde{K}]$. By substituting the discretized form of $\{\dot{\overline{u}}\}_{t+\Delta t}$ and $\{\ddot{\overline{u}}\}_{t+\Delta t}$ into the recurrence Eq. (2.4.4) and then solving for $\{\overline{u}\}_{t+\Delta t}$, one can obtain the recurrence formula in terms of effective stiffness and effective load vector.

$$[K^*]\{\overline{u}\}_{t+\Delta t} = \{\overline{F}^*\}_{t+\Delta t} \qquad (2.4.5)$$

where the effective stiffness matrix is:

$$[K^*] = [K] + \frac{\gamma}{\Delta t\beta}[\tilde{C}] + \frac{1}{\Delta t^2\beta}[M] \qquad (2.4.6)$$

26

The effective load vector is:

$$\{\bar{F}^*\}_{t+\Delta t} \tag{2.4.7}$$

$$= \{\bar{F}\}_{t+\Delta t} + \left[\tilde{C}\right]\left[\frac{1}{\Delta t\beta}\{\dot{\bar{u}}\}_t + \left(\frac{\gamma}{\beta} - 1\right)\{\dot{\bar{u}}\}_t + \frac{\Delta t}{2}\left(\frac{\gamma}{\beta} - 2\right)\{\ddot{\bar{u}}\}_t\right]$$

$$+ [M]\left[\frac{1}{\Delta t^2\beta}\{\dot{\bar{u}}\}_t + \frac{1}{\Delta t\beta}\{\dot{\bar{u}}\}_t + \left(\frac{1}{2\beta} - 1\right)\{\ddot{\bar{u}}\}_t\right] + [M]$$

In Eq. (2.4.5) $\{\bar{u}\}_{t+\Delta t}$ is unknown, and is calculated by solving the linear equation

numerically. In many cases, one can implement an LU decomposition method in order to

solve the linear system. However, if the size of the matrices is very large, one could use a

method that substructures the matrices such as banded or skyline solver.

Once the solution for the displacement vector is obtained, one can use Eq. (2.4.2) and Eq.

(2.4.3) to calculate the solution for velocity and acceleration at time $t + \Delta t$.

2.5 Chapter Summary

This chapter presents a model for acoustic wave propagation in a pipe–like domain.

Acoustic mass and stiffness matrices are derived from the kinetic and potential energy

while the impedance damping and stiffness matrices are derived from the prescribed

acoustic impedance. Solving the Lagrange equations and incorporating boundary

conditions yield the equations of motion for wave propagation. Since the field variable is

the acoustic displacement, a brief post–processing section is also presented, which

explains how to obtain the acoustic pressure from the acoustic displacement. In addition,

a section on time integration to solve the equations of waves provides a brief review on the Newmark method.

CHAPTER 3   ACOUSTIC MODEL RESULTS

This chapter presents the implementation of the FE-Ritz method for acoustic wave propagation inside a prismatic pipe and the results in both time and space domain. These results are compared with their corresponding analytical solutions. Also, this chapter presents the acoustic pressure results in time domain and space domain for a one-sixth sector of a fuel bundle and full fuel bundle along with their corresponding numerical validation. Lastly, the FE – Ritz method is used to study the sound propagation through the sub-channel system when it is generated at one discrete location. A graphical post-processing tool was also developed in order to generate the spatial domain plots for the three-dimensional systems.

3.1   Plane Wave Solution

In order to test the previous FE formulation, one can apply the boundary conditions to model simple systems whose solution is already known. Ideally, if sound were to travel through a pipe with smooth and rigid walls, its behavior would be that of a plane wave. Hence, imposing these conditions to the proposed model should yield the same results as those from a plane wave case. It is assumed that, at the outlet of the system, the wave will interact with a reacting and absorbing wall. The pressure along the pipe is given by Yu and Kawall (2013) as

$$\hat{p}_L(z) = \rho c V_0 \frac{(Z_r + iZ_i) \cos k(L - z) - i \sin k(L - z)}{\cos kL - i(Z_r + iZ_i) \sin kL}$$

$$(3.1.1)$$

29

Eq. (3.1.1) is the analytical solution for the acoustic complex pressure everywhere if the walls of the pipe are smooth and rigid. For this test case, it is not necessary to completely discretize an entire domain, but rather use one element as depicted in Figure 2.1, which essentially models a prismatic pipe.

3.1.1 Prescribed Moving Boundary Source

Sound propagation through an internal domain can be introduced by a prescribed initial condition or can be originated at the boundary. Based on the assumption of no fluid flow, the waves must be produced at a boundary. In order to model an acoustic source at a boundary, one can use a time-varying harmonic function, which could be interpreted as a speaker inducing sound in the system. For example, this boundary condition can be applied at the inlet of the pressure pipe allowing it to vary only with respect to $\bar{w}_e$ as

$$\bar{u}\left(x,y,z\right)|_{\forall N_e(x,y,z=0)} = \begin{Bmatrix} 0 \\ 0 \\ W_{0s} \end{Bmatrix} \sin \omega t \qquad (3.1.2)$$

Applying this condition to Eq. (2.1.1) is the same as prescribing the movement of the inlet nodes, which makes the first coefficients equal to $W_{0s} \sin \omega t$,

$$\bar{u}_{ze}\left(x,y,0\right) = [N_1(\xi,\eta)]_{1X6} \begin{Bmatrix} W_{0s} \sin \omega t + \bar{u}_{z1}0 + \cdots + \bar{u}_{zn}0 \\ W_{0s} \sin \omega t + \bar{u}_{z1}0 + \cdots + \bar{u}_{zn}0 \\ \vdots \\ W_{0s} \sin \omega t + \bar{u}_{z1}0 + \cdots + \bar{u}_{zn}0 \end{Bmatrix}_{6\times3\times(n+1)X1} \qquad (3.1.3)$$

This constraint can be implemented into a force vector through the stiffness and mass matrices by simply substituting the components in all rows and columns that correspond

to the $\bar{u}_{z0}$ coefficient for each node by $W_{0s} \sin \omega t$ and deleting the first row and column.

In brief, this is incorporated into an acoustic force vector defined as

$$\{Q_{zs}\} = \begin{Bmatrix} (K_{2,1} - M_{2,1}\omega^2)W_{0s} \\ (K_{3,1} - M_{3,1}\omega^2)W_{0s} \\ \vdots \\ (K_{6\times3\times(n+1),1} - M_{6\times3\times(n+1),1}\omega^2)W_{0s} \\ 0 \end{Bmatrix} \qquad (3.1.4)$$

Using this force vector modifies the equation of motion as follows

$$[M]\{\ddot{\bar{u}}\} + [\tilde{C}]\{\dot{\bar{u}}\} + ([K] + [\tilde{K}])\{\bar{u}\} = \begin{Bmatrix} 0 \\ 0 \\ \{Q_{zs}\} \end{Bmatrix} \sin \omega t \qquad (3.1.5)$$

3.1.2   Smooth and Rigid Walls

Assuming that the walls of the pipe are smooth and rigid simplifies the behavior of acoustic waves so that the acoustic displacement varies only along the z-axis within one element. This means that the normal displacement with respect to the z-axis at the walls of the prism must vanish. This leads to the following boundary condition:
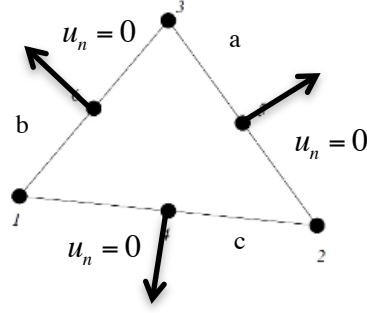
Figure 3.1: Rigid boundary conditions for one prismatic pipe.

$$u_{xa,b,c}\cos\varphi_{a,b,c} + u_{ya,b,c}\sin\varphi_{a,b,c} = 0 \qquad (3.1.6)$$

where a, b and c are the faces of the prism and φ_a, φ_b, φ_c are the normal angles of the corresponding side with respect to the local coordinate system.

Eq. (3.1.6) can also be written in matrix as:

$$\begin{Bmatrix} \bar{u}_{xO} \\ \bar{u}_{xI} \\ \bar{u}_{xO} \end{Bmatrix}_a = \begin{bmatrix} \tan\varphi_a & 0 & 0 \\ 0 & \tan\varphi_a & 0 \\ 0 & 0 & \tan\varphi_a \end{bmatrix} \begin{Bmatrix} \bar{u}_{yO} \\ \bar{u}_{yI} \\ \bar{u}_{yO} \end{Bmatrix}_a \qquad (3.1.7)$$

$$\begin{Bmatrix} \bar{u}_{xO} \\ \bar{u}_{xI} \\ \bar{u}_{xO} \end{Bmatrix}_b = \begin{bmatrix} \tan\varphi_b & 0 & 0 \\ 0 & \tan\varphi_b & 0 \\ 0 & 0 & \tan\varphi_b \end{bmatrix} \begin{Bmatrix} \bar{u}_{yO} \\ \bar{u}_{yI} \\ \bar{u}_{yO} \end{Bmatrix}_b$$

$$\begin{Bmatrix} \bar{u}_{xO} \\ \bar{u}_{xI} \\ \bar{u}_{xO} \end{Bmatrix}_c = \begin{bmatrix} \tan\varphi_c & 0 & 0 \\ 0 & \tan\varphi_c & 0 \\ 0 & 0 & \tan\varphi_c \end{bmatrix} \begin{Bmatrix} \bar{u}_{yO} \\ \bar{u}_{yI} \\ \bar{u}_{yO} \end{Bmatrix}_c$$

Or

$$\left\{\bar{u}_x\right\}_a - [R]_a\left\{\bar{u}_y\right\}_a = 0, \left\{\bar{u}_x\right\}_b - [R]_b\left\{\bar{u}_y\right\}_b = 0, \left\{\bar{u}_x\right\}_b - [R]_b\left\{\bar{u}_y\right\}_b = 0 \quad (3.1.8)$$

where I and O subscripts represent the interior and corner nodes, respectively.

These constraints can be implemented into an augmented Lagrangian, which is used in a method of Lagrange multipliers to account for the constraint forces at the boundary, and established the set of partial differential equations of wave propagation. This is achieved this by introducing the following potential to the Lagrangian

$$L^* = \left\{\left\{\bar{u}_x\right\}_a - [R]_a\left\{\bar{u}_y\right\}_a\right\}^T \{\lambda_a\} + \left\{\left\{\bar{u}_x\right\}_b - [R]_b\left\{\bar{u}_y\right\}_a\right\}^T \{\lambda_b\} + \left\{\left\{\bar{u}_x\right\}_c - [R]_c\left\{\bar{u}_y\right\}_c\right\}^T \{\lambda_c\} \quad (3.1.9)$$

The Lagrangian with this potential is now the so-called augmented Lagrangian where $\{\lambda_a\}$, $\{\lambda_b\}$ and $\{\lambda_c\}$ represent the constraint forces on the faces of the prism. Incorporating the work done by the constraint forces at the boundary of the pipe, the equations of motion Eq. (3.1.5) takes the form

$$[M]_g\{\ddot{\bar{u}}\}_g + [C]_g\{\dot{\bar{u}}\}_g + [K]_g\{\bar{u}\}_g = \begin{Bmatrix} 0 \\ 0 \\ \{Q_{zs}\} \end{Bmatrix} \sin\omega t \qquad (3.1.10)$$

Note that Eq. (3.1.10) accounts only for the axial displacement $\{\bar{u}_z\}$, which is expected by virtue of the applied boundary conditions.

This method can be further used for implementing interfacial boundary conditions for models with multiple flow-sections or to account for bundle misalignment.

3.1.3 Plane Wave Results

Numerical results are compared against the analytical solution in both the space and time domain, where the space domain illustrates the steady state solution of the system after iteration time and the time domain illustrates the time response for the acoustic pressure.

Within one FE-Ritz element, the plane wave results in Figure 3.2 and Figure 3.3 are calculated using the following parameters:

Table 3.1: Values of Geometric Properties Used for Plane Wave Test Case in Air.

Parameters	
Density $\rho \left(\frac{kg}{m^3}\right)$	1.2
Length L (m)	1.705 m
Speed of sound c $\left(\frac{m}{s}\right)$	341 m/s
Piston velocity V_0 $\left(\frac{m}{s}\right)$	0.01 m/s
Real acoustic impedance Z_R	4
Imaginary acoustic impedance Z_I	3
Excitation frequency ω $\left(\frac{rad}{s}\right)$	270
Time step	0.001 sec
Total time	0.2 sec
Order of polynomial n	5
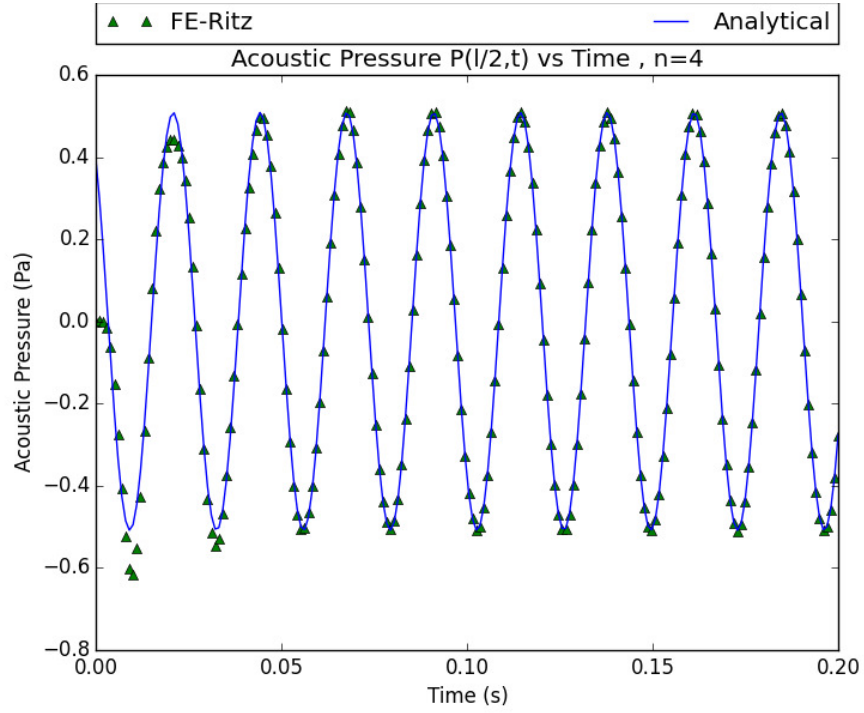
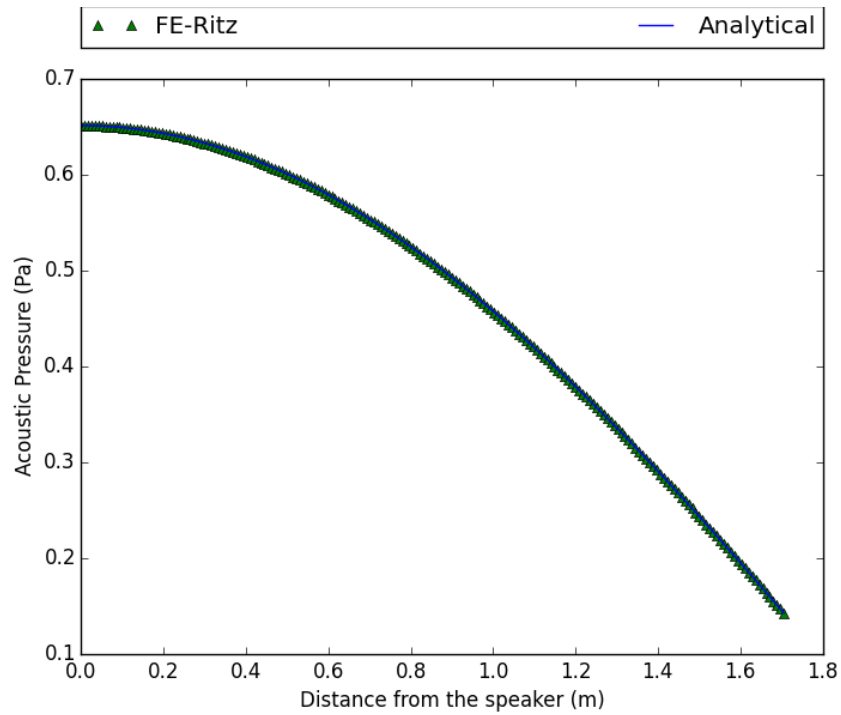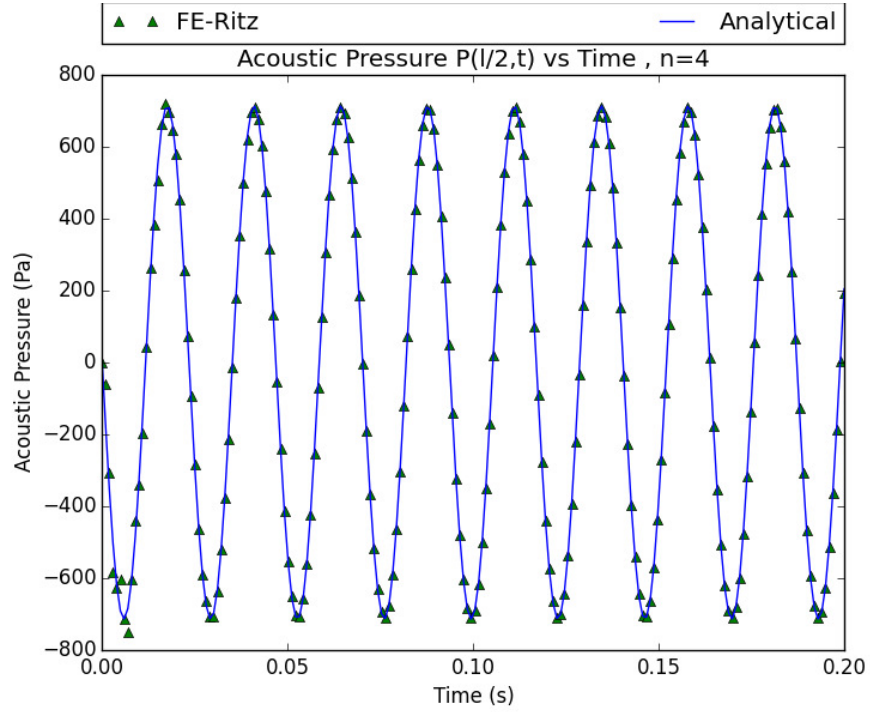*Figure 3.2: Time domain response of FE-Ritz method for plane wave test case in air.*

Figure 3.3: Steady state acoustic pressure for plane wave test case in air.

The results shown in Figure 3.4 and Figure 3.5 are found from the parameters in the case of a pipe filled with water.

Table 3.2: Values of Geometric Properties Used for Plane Wave Test Case in Water

Parameters	
Density ρ $\left(\frac{kg}{m^3}\right)$	1000.0
Length L (m)	$1.705\ m$
Speed of sound c $\left(\frac{m}{s}\right)$	$1500\ m/s$
Piston velocity V_0 $\left(\frac{m}{s}\right)$	$0.01\ m/s$
Real acoustic impedance Z_R	0.5
Imaginary acoustic impedance Z_I	7.50
Excitation frequency ω $\left(\frac{rads}{s}\right)$	270
Time step	0.001 sec
Total time	0.2 sec
Order of polynomial n	5

Figure 3.4: Time domain response of FE-Ritz method for plane wave test case in water
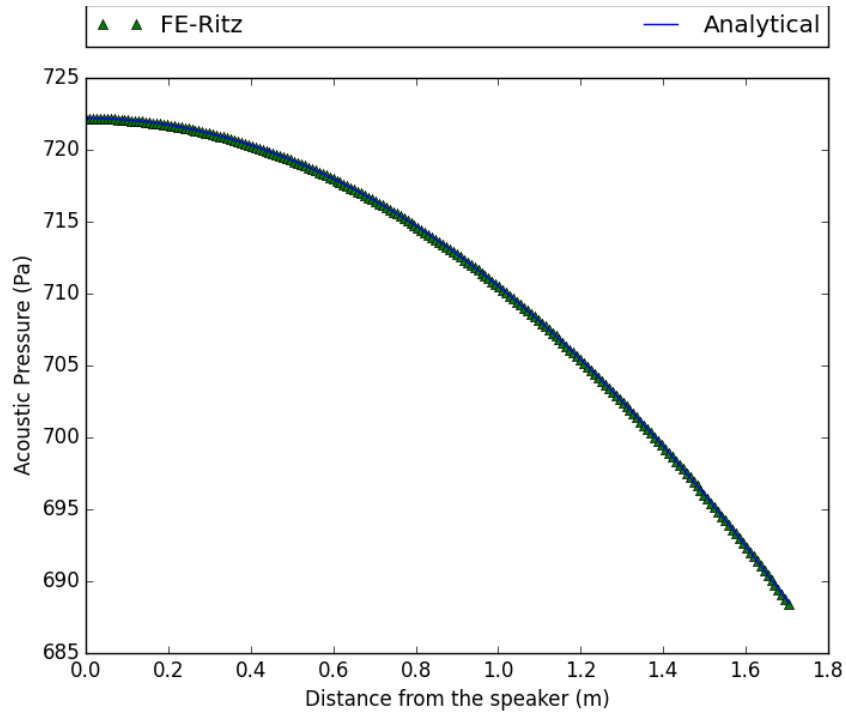
Figure 3.5: Steady state acoustic pressure for plane wave test case in water.

In Figure 3.2 - Figure 3.5, it can be seen that both the analytical and numerical solution are in excellent agreement.

The time domain results in Figure 3.2 and Figure 3.4 show that the computed solution reaches steady state within the first three cycles of oscillations; hence the computed responses are phase-shifted in order to numerically compare the results against the analytical solution. The acoustic impedance for both water and air are arbitrarily calculated based on the media in which sound propagates and then stiffness and damping characteristics of the material at the outlet. Further, based on the speed of the wave, the time step is chosen in order to use at least 10 points per period to capture time domain variation.

3.2 Verification of Acoustic Waves in Coherent Sub-Channel Systems

This section presents the results obtained from the plane wave test case within one prism element and the results for a global system that simulates the propagation of acoustic waves throughout a one-sixth sector, Figure 3.6, of the cylindrical domain depicted in Figure 1.2.

The symmetry of the fuel channel can be used to further reduce the computational time since the number of elements required to mesh a sector domain is less than the number of elements required to mesh the entire cross-section. Moreover, a meshing criteria needs to be satisfied given that, in order to capture small fluctuations, one would require a minimum number of nodes per wavelength. The number of nodes is proportional to the

wave number of the medium. In this case, the medium is water and applying an induced frequency of 80 Hz for which the wave number is 0.3 or of 30 m wavelength, would require at least 6 nodes per wavelength and a 3rd order polynomial.
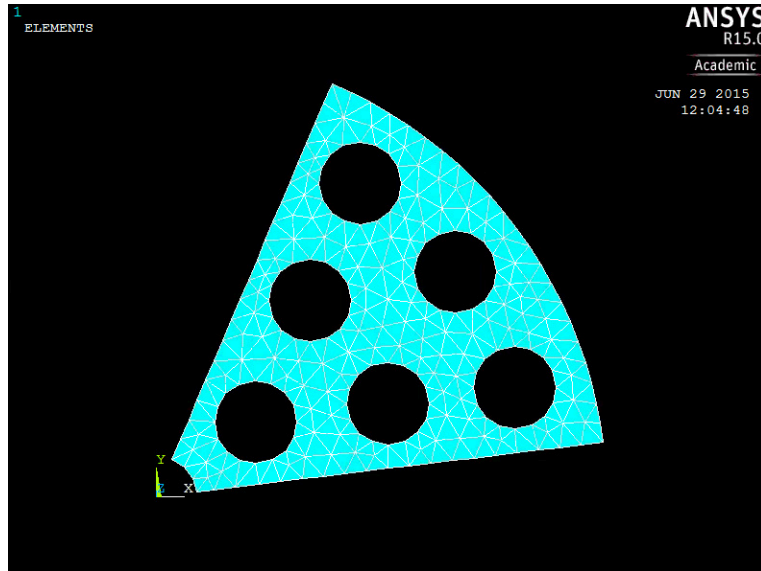

Figure 3.6: Cross-section mesh for sector domain.

3.2.1 Acoustic Wave Propagation in a Sector of Fuel Channel

The following results are computed using the parameters in Table 3.3 for the assumptions stated in Chapter 1 and in a fraction of the domain depicted in Figure 1.2. The numerical results are then compared against numerical results obtained from ANSYS for a model with the same characteristics.

Table 3.3: Values of Geometric Properties for Global System.

Parameters	
Density $\rho \left(\frac{kg}{m^3}\right)$	1000
Length L (m)	0.5 m
Radius r (m)	0.06
Piston pressure on inlet area P_0 $\left(\frac{Kgm}{s^2}\right)$	$5 \frac{Kgm}{s^2}$
Real acoustic impedance Z_R	4
Imaginary acoustic impedance Z_I	0
Excitation frequency ω $\left(\frac{rad}{s}\right)$	$500 \frac{rad}{s}$
Time step	0.00001 sec
Total time	0.1 sec
Order of polynomial n	5

Figure 3.7 to Figure 3.12 depict the cross-section pressure distribution at different

locations along the pipe after 0.1 seconds computed with the FE-Ritz method. Figure 3.13

depicts the space steady state space domain solution of the pressure distribution along the

pipe. Figure 3.14 shows the comparison between the FE-Ritz model and the ANSYS

model in time-domain.
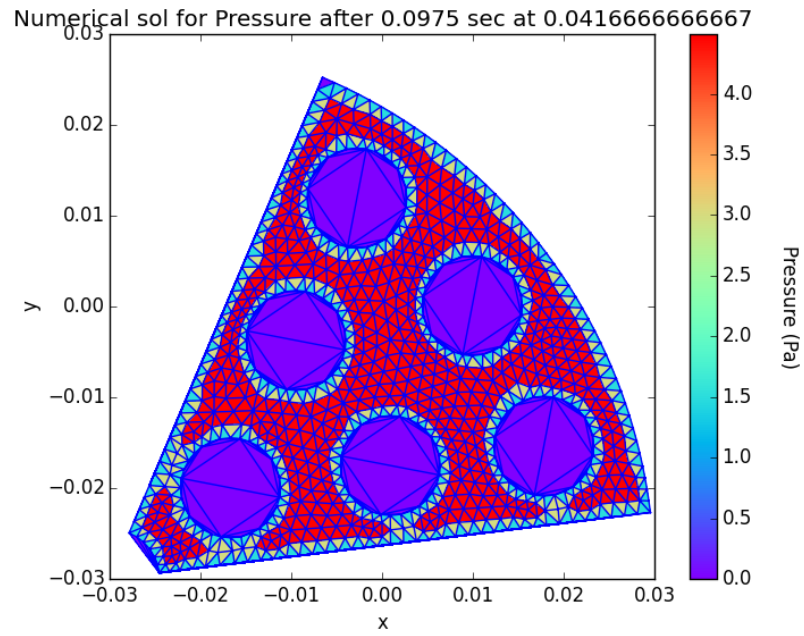
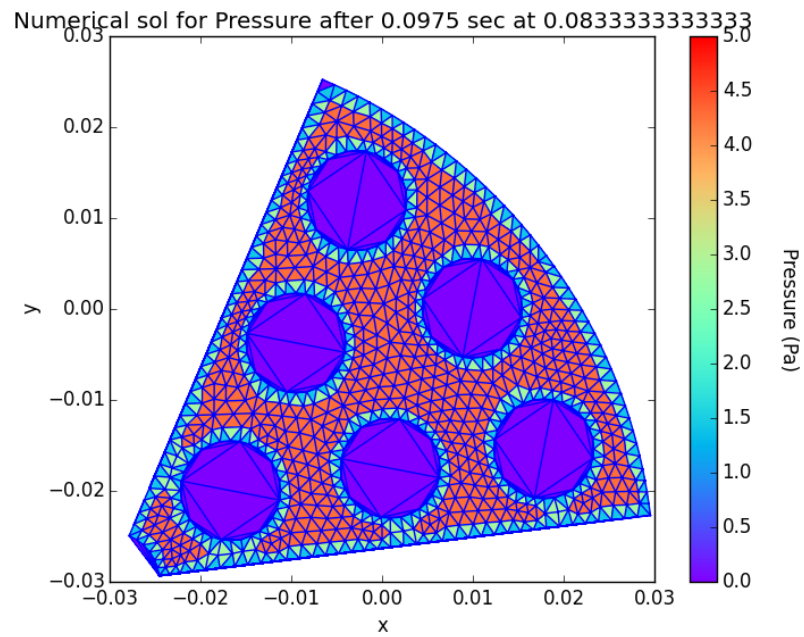*Figure 3.7: Cross-section pressure at different z location: L/12*

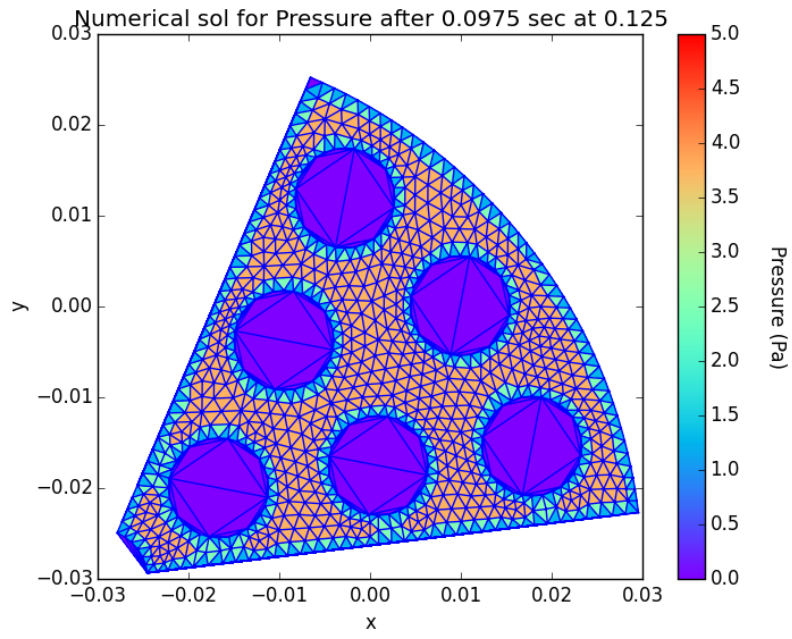*Figure 3.8: Cross-section pressure at different z location: L/8*

41

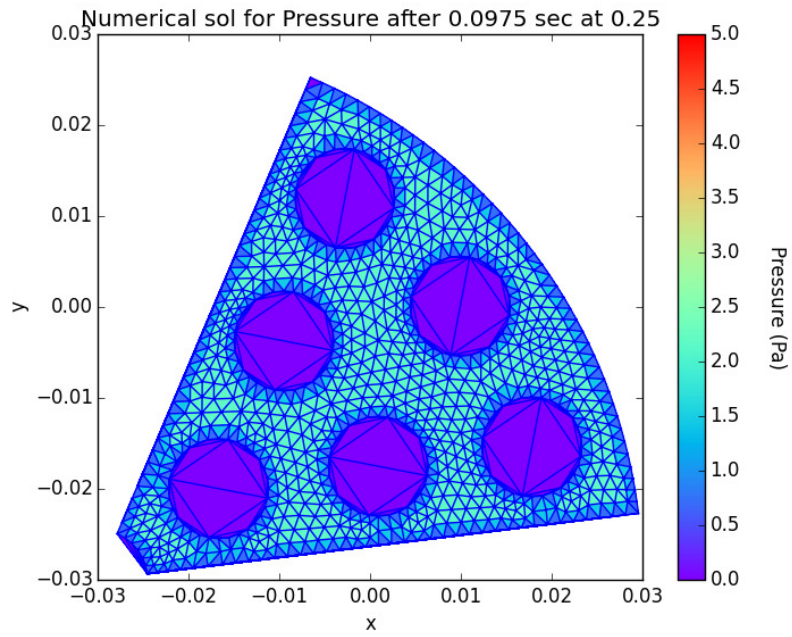*Figure 3.9: Cross-section pressure at different z location: L/4.*

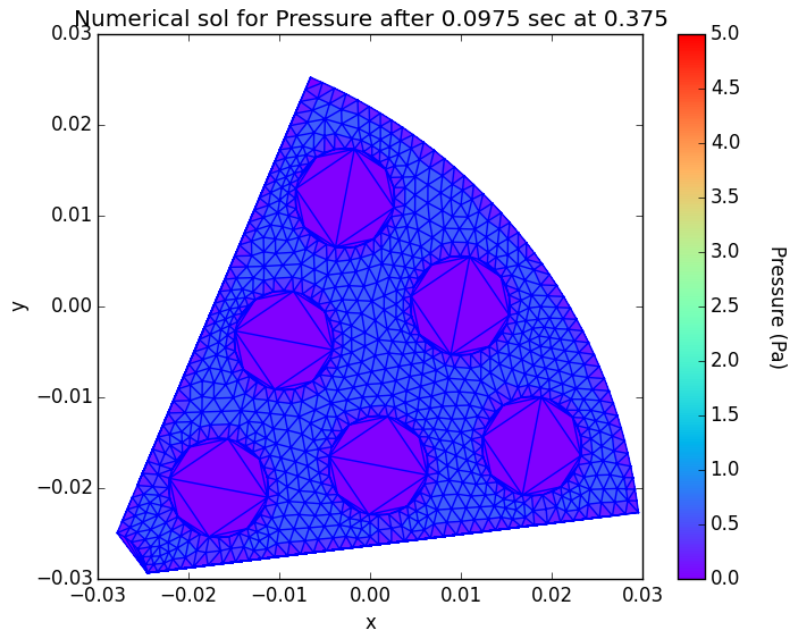*Figure 3.10: Cross-section pressure at different z location: L/2.*

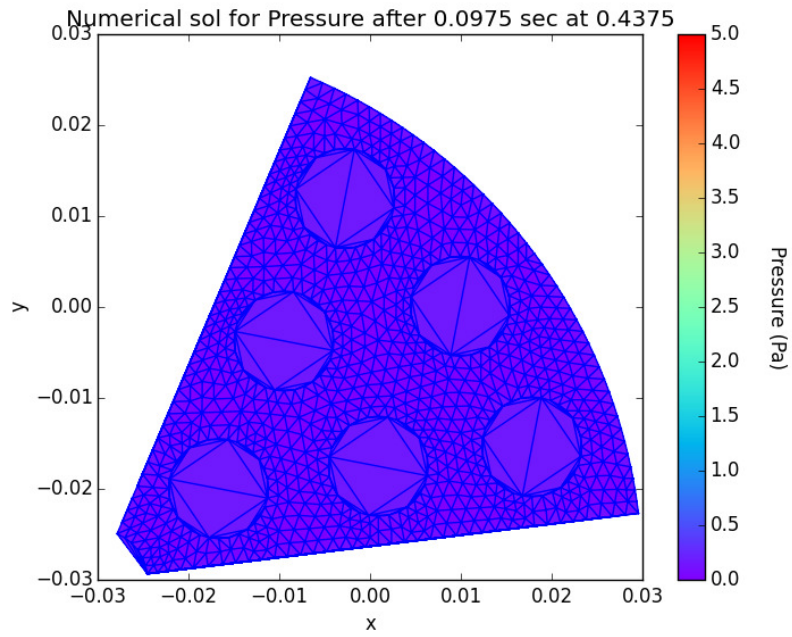*Figure 3.11: Cross-section pressure at different z location: 3L/4.*

Figure 3.12: Cross-section pressure at different z location: 7L/8.

The induced pressure at the inlet has a magnitude of 5 Pa. In order to validate these results, an ANSYS model was generated using 8-node acoustic brick elements. The same parameters and physical dimensions are applied after manipulating the global matrices to fit the boundary conditions. The generated matrices have a dimension of (8910 by 8910) with a 2D mesh of 379 elements with 912 nodes. With this in mind, using Python's libraries to solve the system of equations and time integrating for 10000 steps takes approximately 10 minutes to yield a solution in a 2.6 GHz Intel Core i5 machine with 8 GB or RAM. On the other hand, the 3D ANSYS model has 10860 low order elements with 14511 and it takes approximately 30 minutes to yield a solution when computed in a machine with a 2.67 GHz Inter Xeon processor and 16 GB or RAM.
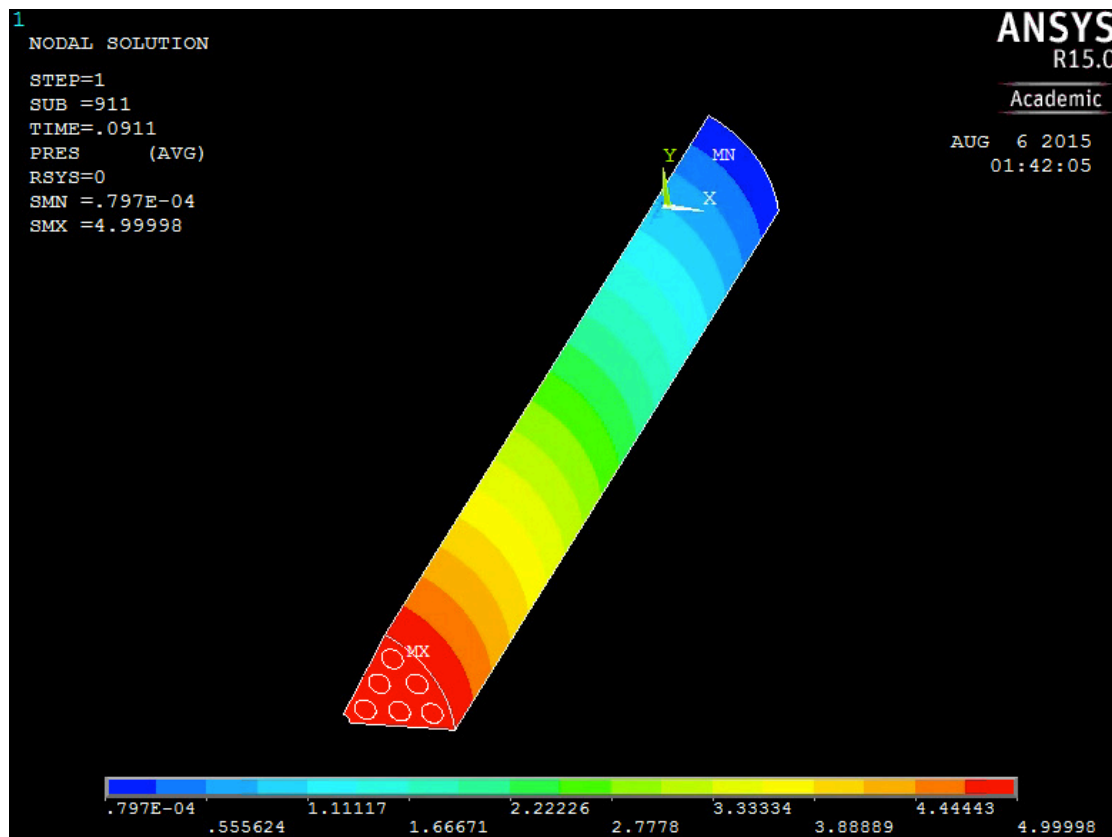

Figure 3.13: ANSYS Model, Steady state for pressure distribution along sector.

44

For simplicity, the boundary condition is prescribed so that all walls along the pipe are considered to be smooth and rigid. Also, similar to the plane wave test case, the inlet is in contact with a piston or a loud speaker that generates the acoustic pressure and the outlet is made up of a reacting and acoustic material with prescribed acoustic impedance.
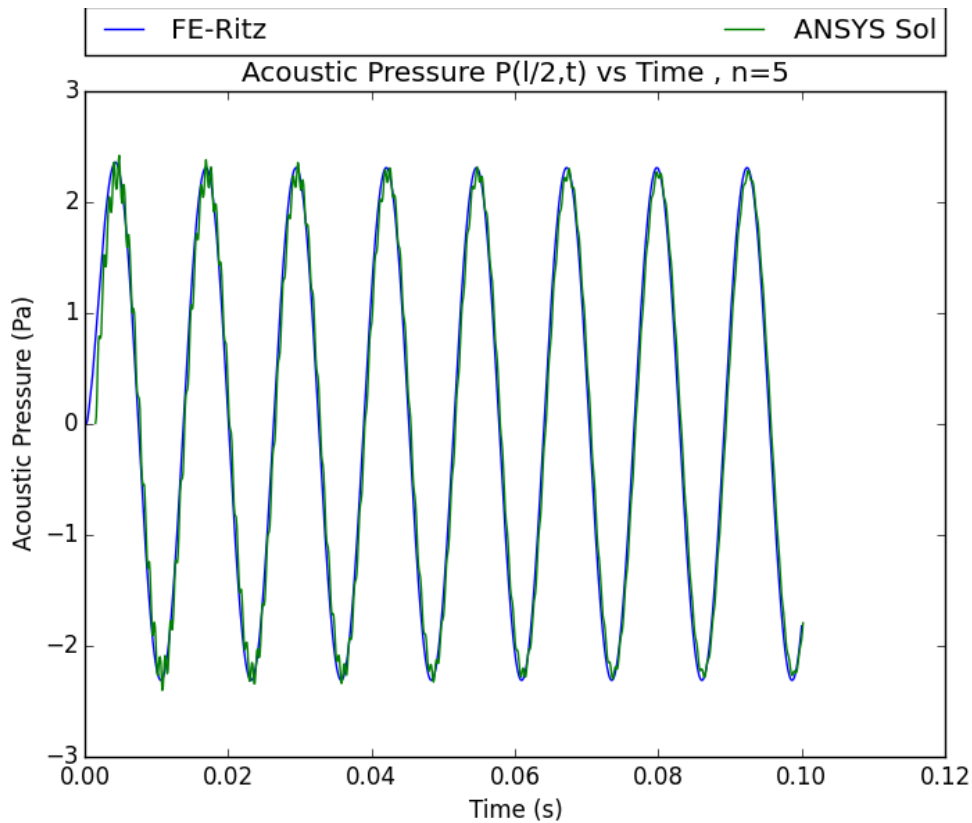

Figure 3.14: Time domain response for one node located at L/2 (FE-Ritz vs. ANSYS).

The results depicted in Figure 3.7 - Figure 3.12 are within the same range of values at the corresponding cross-section when compared to the results in Figure 3.13. Further, the results in Figure 3.14 appear to be shifted by a phase angle. This is because the results from ANSYS converge after 4 cycles due to the low order element (8-node bricks) used, while the FE-Ritz method achieves steady state within the first 2. This can also be noticed

45

at the peak of the ANSYS response, which shows some noise within the first cycles that is then smoothed out in the last cycle.

3.2.2 *Acoustic Wave Propagation in Full Fuel Channel*

The sector model reduces the degrees of freedom and computational time by using the periodicity or symmetry of the bundle. However, the sector results may only be used if one were to apply symmetric boundary conditions so that obtaining results for the whole bundle would be a matter of rotation.

An advantage of the FE-Ritz method is flexibility of reducing the degrees of freedom without affecting the solution by using a low order polynomial, if appropriate. In water, the speed of sound is 1500 m/s. If the speaker at the inlet has an excitation at a frequency of 80 Hz, the resulting wavelength is approximately 19 m. Ideally, one is able to capture the wave using three points per wavelength. Therefore, a third order polynomial is also able to capture the wave traveling along a 50 cm bundle which reduces the computational time, making it possible to model the entire bundle.

Figure 3.15 to Figure 3.19 are snapshots taken a different cross-sections computed with the FE-Ritz method for the same parameters as in Table 3.3.
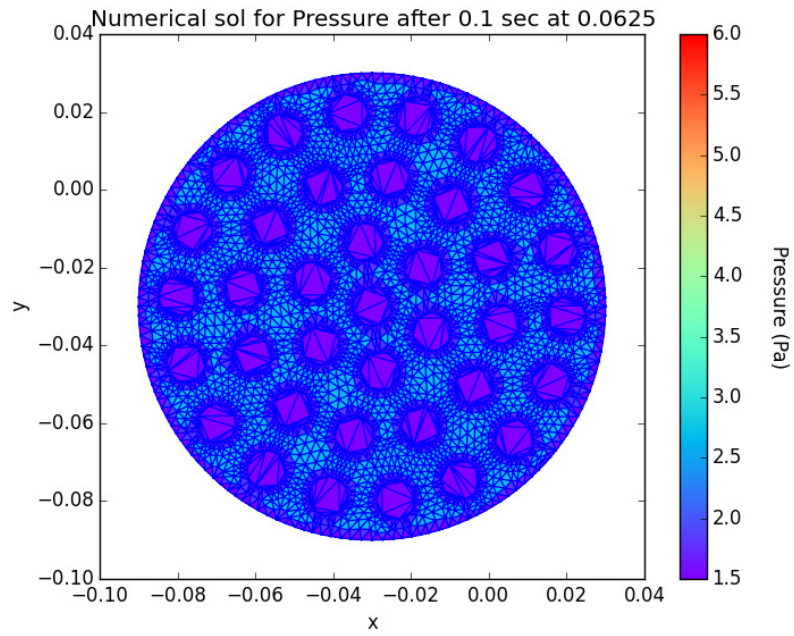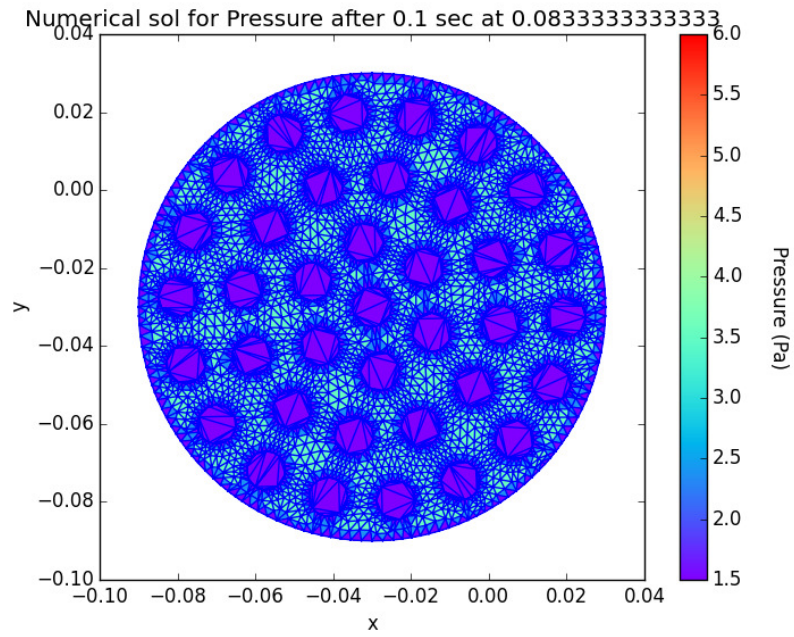
Figure 3.15: Cross-section pressure at z=L/8.
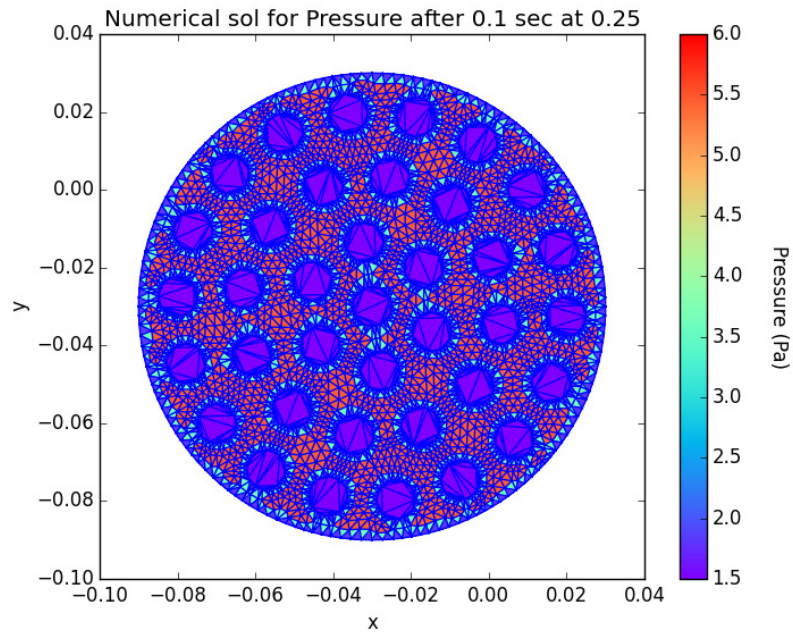

Figure 3.16: Cross-section pressure at z=L/4.
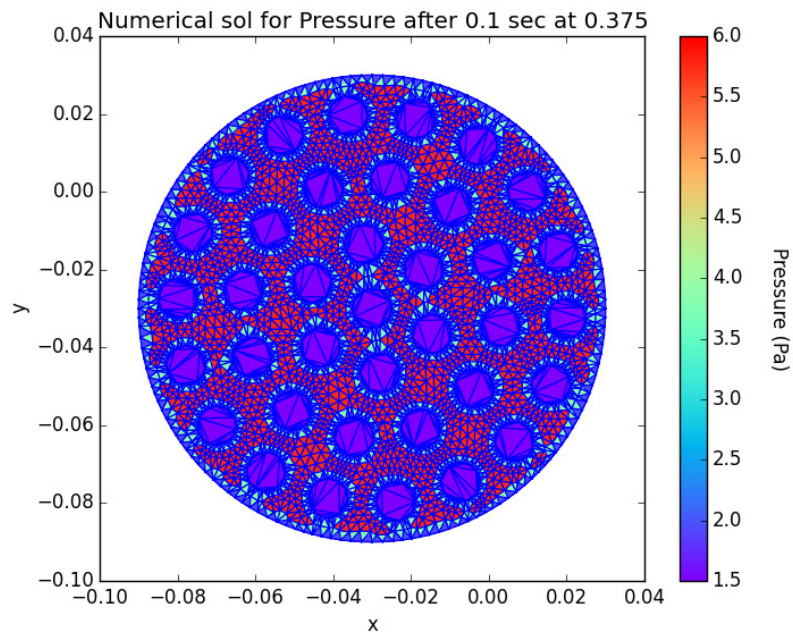
Figure 3.17: Cross-section pressure at z=L/2.
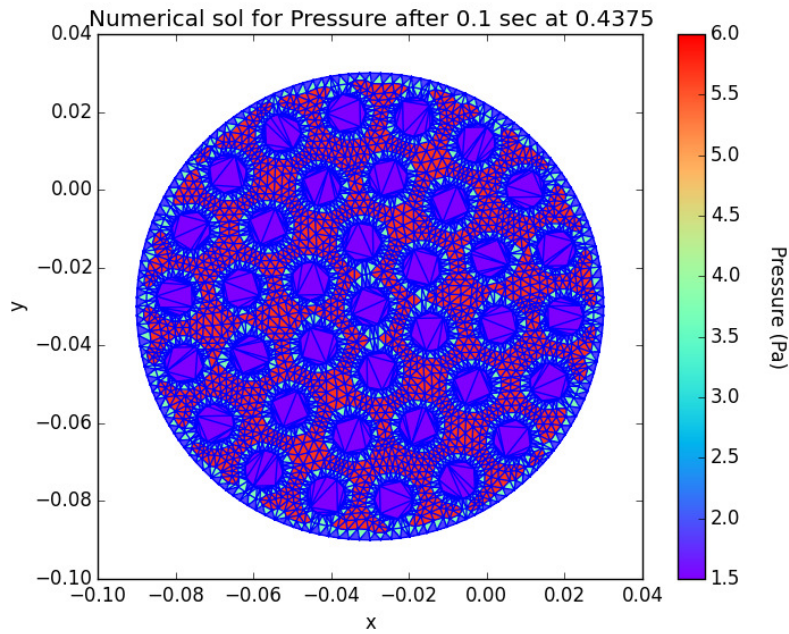

Figure 3.18: Cross-section pressure at z=3L/4.

Figure 3.19: Cross-section pressure at z=7L/8.

Since the pressure distribution on the cross-section reaches steady state after a couple of coalitions, one can obtain an idea of the pressure distribution for acoustic wave along the bundle by plotting the steady state for an arbitrary node, as shown in Figure 3.20.
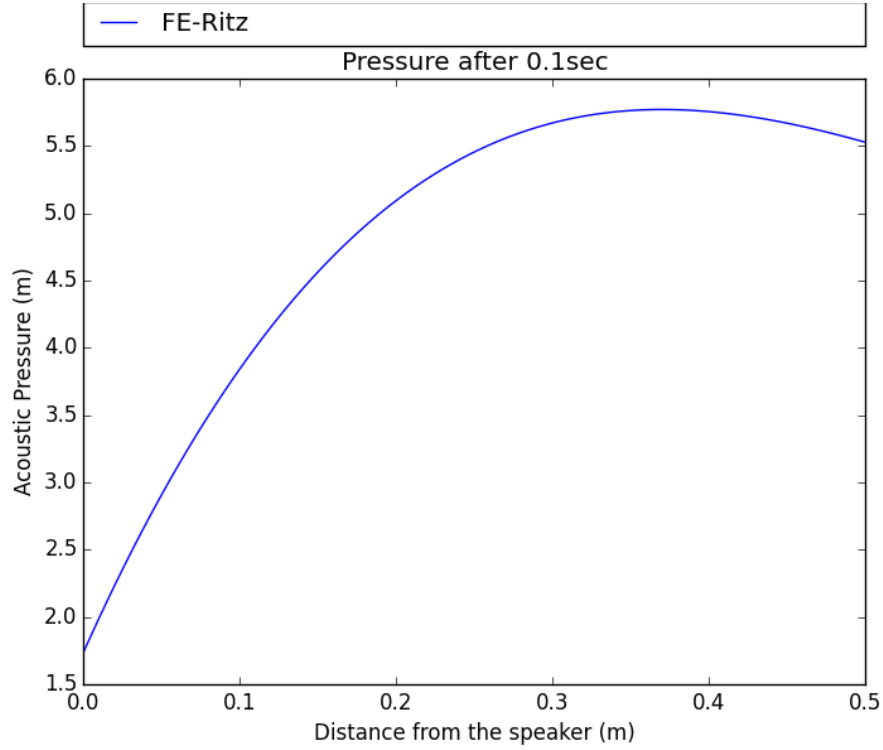
Figure 3.20: Steady state acoustic pressure for arbitrary node after 0.1 sec.

Note that the peak pressure increases along the pipe up to 0.3 m and then decreases at a slower rate. This is due to the acoustic impedance used for this specific case. The prescribed acoustic impedance makes the boundary slightly absorbent.

3.2.3   Point Source in Sector

The following test case is presented in order to observe the development of an acoustic burst inside the pressure pipe, as shown in Figure 3.21. The system resembles the same characteristics as previous examples with the exception of a point source located in the middle of the domain. A time-harmonic source is also prescribed at the inlet to achieve steady state, once the initial source has disappeared. The following figures were

generated with an earlier version of the post-processing module, in which the element triangulation was not very compatible with 6-node triangular elements. Nevertheless, one is able to observe the wave propagation through the coherent sub-channel system as the wave travels along the pressured pipe.
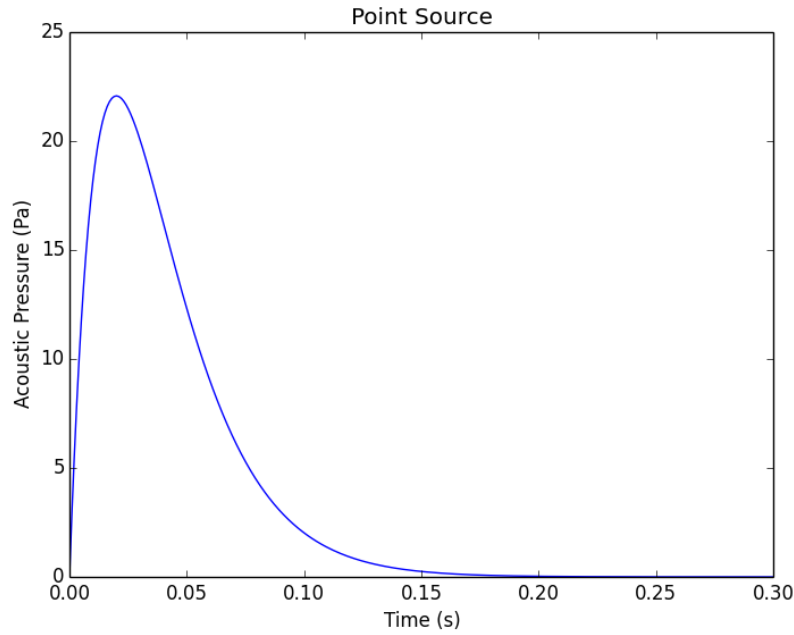

Figure 3.21: Burst function at 0.02 sec.

In finite element, this burst function is implemented by exciting one node with a constant force, which then decreases over time as governed by the following equation:

$$B(t) = A_0 t e^{-\omega_b t} \tag{3.2.1}$$

For this test case, the parameters in Table 3.*4* are used.

51

Table 3.4: Values of Geometric Properties for Burst Test Case.

Parameters	
Density $\rho \left(\frac{kg}{m^3}\right)$	1000
Burst amplitude (Pa)	3000 (Pa)
Length L (m)	0.01 m
Radius r (m)	0.06
Piston pressure on inlet area P_0 $\left(\frac{Kgm}{s^2}\right)$	$5 \frac{Kgm}{s^2}$
Real acoustic impedance Z_R	4
Imaginary acoustic impedance Z_I	0
Excitation frequency ω $\left(\frac{rad}{s}\right)$	$270 \frac{rad}{s}$
Burst frequency $-\omega$ $\left(\frac{rad}{s}\right)$	$50 \frac{rad}{s}$
Time step	0.0001 sec
Total time	0.3 sec
Order of polynomial n	5

Figure 3.22 to Figure 3.27 depict the pressure distribution on a sector cross-section at 0.005m away from the inlet for different times:
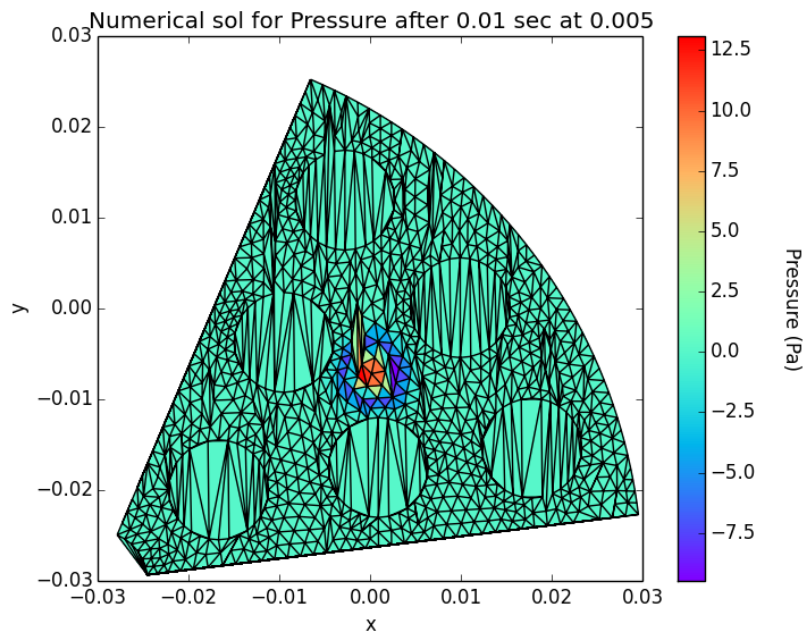
Figure 3.22: Cross-sections at 0.01.
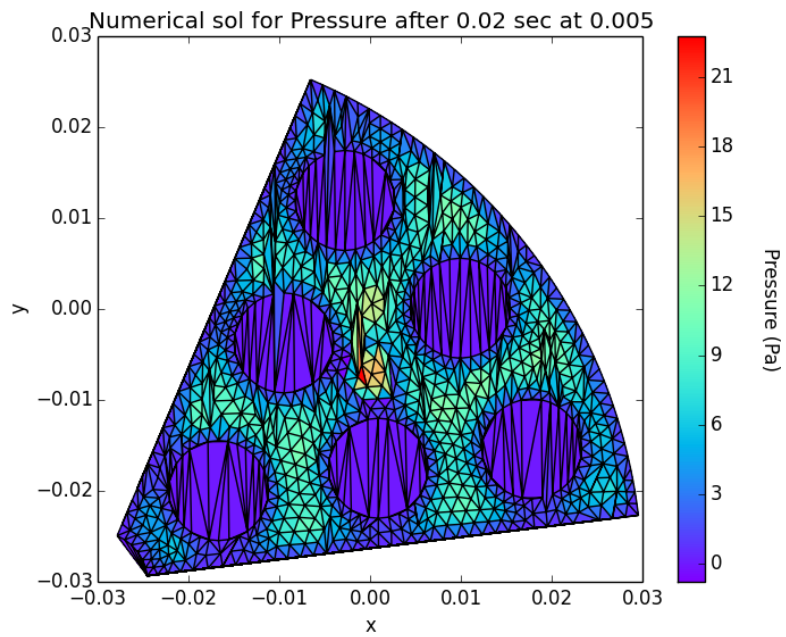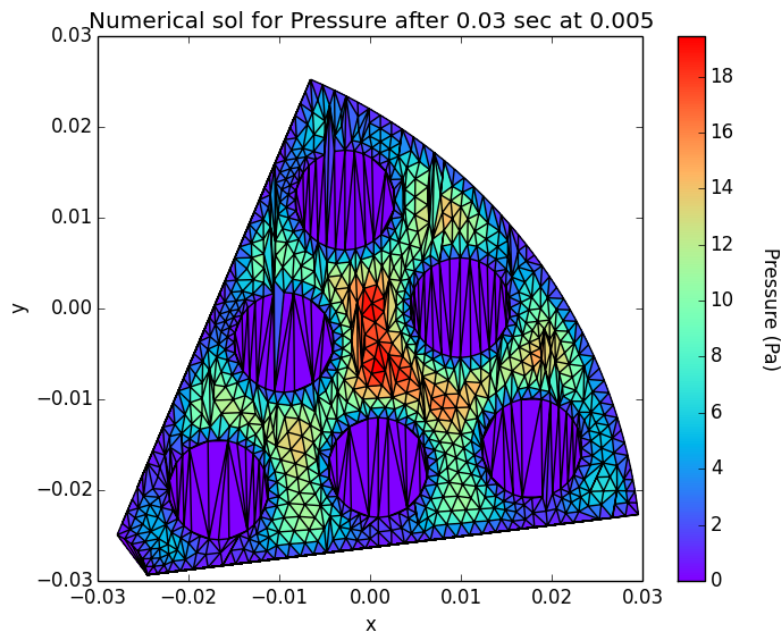

Figure 3.23: Cross-sections at 0.02 sec.
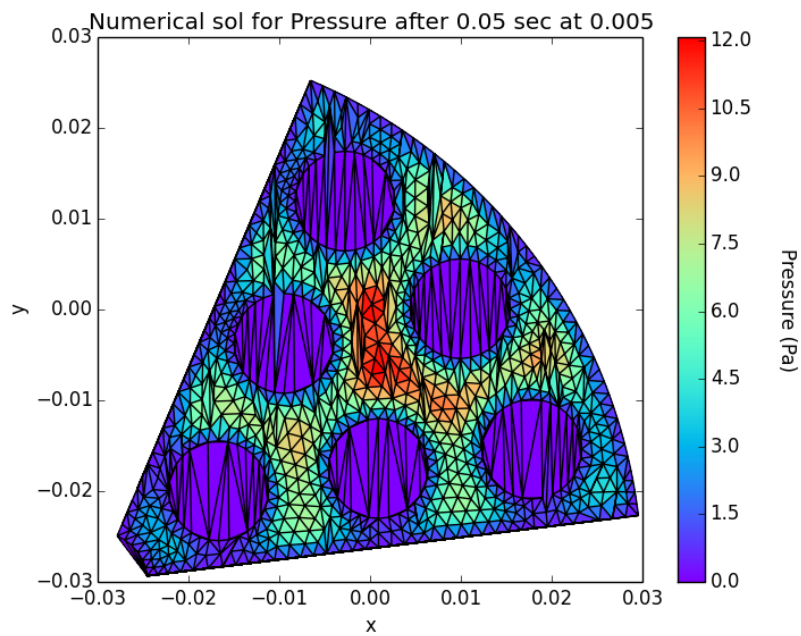
Figure 3.24: Cross-sections at 0.03 sec.

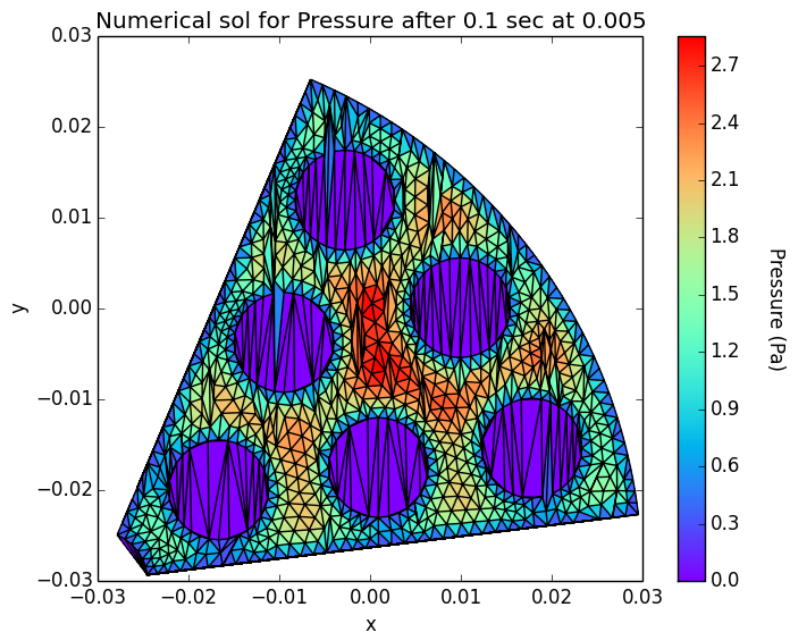*Figure 3.25: Cross-sections at 0.05 sec.*

Figure 3.26: Cross-sections at 0.1 sec.
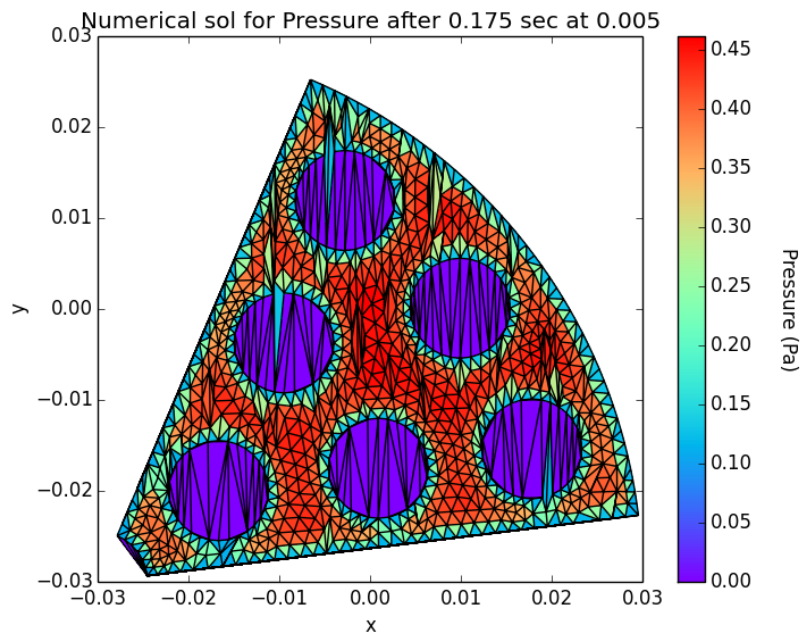
Figure 3.27: Cross-sections at 0.175 sec.

55

The previous figures illustrate how the initial acoustic source propagates through the medium consisting of various sub-channels and walls. One can observe the maximum burst at 0.02 seconds in Figure 3.23 and its decay in Figure 3.24 to Figure 3.27. Moreover, the pressure burst is produced while the speaker is also producing noise, which is why the response at 0.175 sec begins to look like the response in the previous test cases.

3.3   Chapter Summary

This chapter presents the results obtained from the FE – Ritz acoustic model for: 1D plane wave propagation inside a prismatic pipe, 3D wave propagation in a one-sixth sector of a fuel channel and the full fuel bundle channel systems. Furthermore, results for point source propagation in a one-sixth sector are also presented, from which one can observe the propagation of the acoustic wave through the sub-channel system. The results for the 1D plane wave propagation are compared with its corresponding analytical solution and shows very good agreement. The one-sixth sector is also modeled in ANSYS in order to validate the numerical results of the FE – Ritz model. The results from the FE – Ritz model agree with those obtained from ANSYS, showing smaller transient solution and accurate results.

CHAPTER 4   DISCUSSION AND CONCLUSION

A combination of Finite Element method and Ritz method is employed to develop a 3D acoustic model suitable for studying the propagation of acoustic waves in pipe-like domains at low acoustic frequencies. This thesis presented the contributions and results:

- The FE – Ritz method is able to model 3D acoustic waves and can facilitate the simulation of bundle vibration due to acoustic induced vibration.

- Taking advantage of the geometry of elongated systems, the FE-Ritz method is able to reduce computation time and reduce the duration of the transient solution.

- The use of acoustic displacement as the field variable facilitates the implementation and other boundary condition in the system, making the acoustic model highly compatible with other methods and models.

- The acoustic behavior of fluid particles inside a pressured prism-shape pipe is investigated using the combined of FE-Ritz acoustic model. The results in Figure 3.2 to Figure 3.5 depict the pressure response in time domain and space domain. These results also depict the comparison against the analytical solution for the real part of acoustic pressure in Eq. (3.1.1), which validates the results for a plane wave within one element or in one prismatic pipe.

- The FE-Ritz method is also used to study the acoustic wave propagation in both one-sixth-sector domain and the full domain of a CANDU fuel channel. The results are compared against their corresponding numerical ANSYS results from Figure 3.7 to Figure 3.14, for which they are found to be in agreement. Moreover,

the results yielded by the FE-Ritz based model are computed in one third of the time when compared to the ANSYS computation for the one-sixth-sector domain.

- The acoustic pressure response in a CANDU fuel channel is also computed and its results are depicted in Figure 3.15 to Figure 3.20, which show the cross-sectional steady state repose at different locations along the pipe and the pressure distribution along the pipe. Although the main purpose of the research is to model the acoustic wave propagation in a CANDU fuel channel, the method allows a wide range of applications at a cheap computational expense.

- Since the main form of excitation in the first three cases is a time-harmonic source at the inlet, the pressure distribution appears constant at every cross-section throughout the pipe. In order to see a pressure gradient on a cross-section, the last test case deals with a pressure burst at a node. This is essentially a point source that peaks at a specific time and quickly decays. The pressure burst is only applied to a node while the speaker produces the harmonic excitation previously seen in the other test cases. The results are depicted in Figure 3.22 to Figure 3.27 and they show the propagation of the wave as it develops outwards from the center of the domain. Since the burst quickly decays, the response that is obtained at the end is similar to the response of the previous test cases.

The procedure presented in this paper has been implemented into a Fortran 77 code and a Python/C++ code in order to facilitate its use for a wide range of applications including the bundle vibration problem of the CANDU system. Additionally, the analysis done by the code has been proven to be faster than the analysis done by a regular 3D finite

element module, simply because the FE-Ritz method reduces the degrees of freedom and therefore requires less memory and CPU. Further research can be done to solve structure-acoustic interaction problem. In brief, this research accomplished the development of an efficient and accurate method to model 3D acoustic and it has shown results, which validate the method and its implementation.

4.1   Future Work and Recommendations for Improvement

The fuel rods in the CANDU system can acoustically resonate because of the amplification of acoustic pressure pulsations or simply the presence of the acoustic pressure induced by the feeder pump. The behavior can also be studied with an acoustic-structure interaction model. One of the problems with interaction models is the need for automotive meshing and re-meshing. However, with the FE – Ritz acoustic model, it is possible to move the mesh manually (for one cross-sectional mesh), based on some criteria. This accounts for the displacement of the boundary nodes at discreet regions along the length of the pressure pipe, which would require the implementation of continuous boundary conditions for a couple meshes along the pipe. An example of this can be seen in the case that one is interested in the behavior of a rod or beam inside a pipe filled with a fluid subjected to some low-frequency acoustic excitation. Assuming that the rod demonstrates a first mode response, one would need to divide the system into a couple of meshed regions so that rod displacement is accounted from one mesh to the next.

REFERENCES

Astley, R. J., & Eversman, W, (1971). A finite element formulation of the super element structural analysis (program) modules. *European Shipbuilding, 2*, 21-35

Abbasian, F., Yu, S. D., & Cao, J. (2009). Experimental and numerical investigations of three-dimensional turbulent flow of water surrounding a CANDU simulation fuel bundle structure inside a channel. *Nuclear Engineering and Design*, *239*(11), 2224–2235.

Bernhard, R. J. (1982). Acoustic finite element analysis of duct boundaries. Retrieved from http://lib.dr.iastate.edu/rtd/7026/

Bhattacharya, A., & Yu, S. D. (2012). An experimental investigation of effects of angular misalignment on flow-induced vibration of simulated CANDU fuel bundles. *Nuclear Engineering and Design*, *250*, 294–307.

Bhattacharya, A., Yu, S., & Kawall, G. (2012). An experimental investigation of flow-induced vibration of a 43-element simulation CANDU fuel bundle under confined axial flow. Retrieved from http://www.sites.mech.ubc.ca/~ial/CANCAM/CANCAM/cd-final/documents/0067.pdf

Bhattacharya, A., & Yu, S. D. (2012). Numerical Simulation of Flow Through Nuclear Fuel Bundles With Angular Misalignments. *Journal of Fluids Engineering*, *134*(11), 111101.

Bhattacharya, A., Yu, S. D., & Kawall, G. (2013). Simulation of Unsteady Flow Through a String of CANDU Fuel Bundles in a Pressure Tube. *Nuclear Science and Engineering*, *174*(1), 60–78.

Bhattacharya, A., Yu, S. D., & Kawall, G. (2012). Numerical simulation of turbulent flow through a 37-element CANDU fuel bundle. *Annals of Nuclear Energy*, *40*(1), 87–105.

Craggs, A. (1976). A finite element method for damped acoustic systems: an application to evaluate the performance of reactive mufflers. *Journal of Sound and Vibration*, *48*(3), 377–392.

Craggs, A. (1972). The use of simple three-dimensional acoustic finite elements for determining the natural modes and frequencies of complex shaped enclosures. *Journal of Sound and Vibration*, *23*(3), 331–339.

Crocker, M. J. (1998). Mathematical Theory of Wave Propagation. John Wiley & Sons.

Fish, J., & Belytschko, T. (2007). *First Course in Finite Elements*. Hoboken, NJ, USA: Wiley.

Gladwell, G. M. L. (1966). A variational formulation of damped acousto structural vibration problems. *Journal of Sound and Vibration*, *4*(2), 172–186.

Gladwell, G. M. L., & Zimmermann, G. (1966). On energy and complementary energy formulations of acoustic and structural vibration problems. *Journal of Sound and Vibration*, *3*(3), 233–241.

Hackett, R. M. (1976). Three-dimensional finite-element acoustic analysis of solid rocket motor cavities. *Journal of Spacecraft and Rockets*, *13*(10), 585–588.

Hjelmstad, Keith D. (2005). *Fundamentals of Structural Mechanics*. Secaucus, NJ, USA: Springer.

Misra, A., Pauls, R. E., Vijay, D. K., Teper, W., Lin, T. C., Strzelczyk, A., Hemraj, R. (1994). Acoustic modelling in support of fuel failure investigation in a CANDU nuclear generating station. *ASME-PUBLICATIONS-PVP*, *279*, 99–99.

Onate, E. (2009). *Structural analysis with the finite element method linear statics.* Dordrecht: Springer.

Paidoussis, M. P. (1998). *Fluid-structure interactions: slender structures and axial flow* (Vol. 1). Academic press.

Petyt, M., Koopmann, Gh., & Pinnington, R. J. (1977). The acoustic modes of a rectangular cavity containing a rigid, incomplete partition. *Journal of Sound and Vibration*, *53*(1), 71–82.

Rouben, B., (2005). Basic CANDU Design", University Network for Excellence in Nuclear Engineering,

Wenhui, S., & Manzer, A. M. (2005). CANDU Fuel Performance. *AECL, Shanghai Nuclear Design and Research Institute, Available Online: Https://canteach. Candu. org/Content% 20Library/20054409. Pdf*. Retrieved from https://canteach.candu.org/Content%20Library/20054409.pdf

Yetisir, M., & Fisher, N. J. (1997). Prediction of pressure tube fretting-wear damage due to fuel vibration. *Nuclear Engineering and Design*, *176*(3), 261–271.

Yu, S. D., & Kawall, J. G. (2013). Finite Element Analysis of Sound Transmission Loss in One-Dimensional Solids. *Open Journal of Acoustics*, *3*(04), 110.

Zhang, X., & Yu, S. D. (2011). Large eddy simulation of turbulent flow surrounding two simulated CANDU fuel bundles. *Nuclear Engineering and Design*, *241*(9), 3553–3572.

Zienkiewicz, O. C., & Taylor, R. L. (2005). *The finite element method for solid and structural mechanics*. Butterworth-heinemann.

APPENDIX A

The differential equations governing sound propagation are derived from the combination

of the continuity and momentum equations from fluid mechanics by treating the acoustic

signals as small fluctuating disturbances. In order to derive the governing equations of

motion, one assumes that the processes of sound propagation are quasi-static in a

thermodynamic sense (Crocker, 1998). Consequently, the fluid motion is assumed to be

inviscid and compressible. If the system is assumed to be isolated, one can also assume

that no external forces act on the system. Similarly, temperature is assumed to be constant

throughout the system and thus the fluid density is taken to be only a function of pressure.

Hence, density is barotropic. As a result, the fluid motion is both isentropic and irrational.

The linear governing equations for an acoustic wave in a fluid are obtained from the

equations of conservation of mass, Euler's equation (Newton's second law) and an

isentropic disturbance at constant entropy respectively

$$\rho \ \frac{\partial \vec{v}}{\partial t} = -\nabla p \tag{4.1.1}$$

$$\frac{\partial \rho}{\partial t} + (\nabla \cdot \rho \vec{v}) = 0 \tag{4.1.2}$$

$$\frac{\partial p}{\partial t} = c^2 \frac{\partial \rho}{\partial t} \tag{4.1.3}$$

Where ρ is the fluid density, $\vec{v} = \begin{pmatrix} v_x \\ v_y \\ v_z \end{pmatrix}$ is the velocity vector, p is the total pressure and c

is defined as

$$c^2 = \left(\frac{\partial p}{\partial \rho}\right)_s \tag{4.1.4}$$

Which turns out to be the speed of sound in an ideal fluid at constant entropy per

particle(s) (Crocker, 1998).

Linearization of Eq.(4.1.1) and Eq. (4.1.2) is done by using a small perturbation of the

total pressure as a sum of the reference or ambient pressure and the acoustic pressure

$p = p_0 + p'$ with its corresponding expressions for fluctuation in entropy, fluid

density, $\rho = \rho_0 + \rho'$ and velocity, $\vec{v} = \vec{v}_0 + \vec{v}'$ in which the prime variable includes the

first-order approximation for a general equation of state. Additionally, all $zero^{th}$ order

terms are canceled out completely because the ambient variables should correspond to a

valid state of motion in the system yielding the linearized form of Eq. (4.1.3)

$$\frac{\partial \rho'}{\partial t} + \vec{v}_0 \cdot \nabla \rho' + \rho' \nabla \cdot \vec{v}_0 + \vec{v}' \cdot \nabla \rho_0 + \rho_0 \nabla \cdot \vec{v}'_0 = 0 \tag{4.1.5}$$

For an isentropic fluid, the spatial variation of ambient pressure, density and temperature

are very small. Therefore Eq. (4.1.3) can be simplified to

$$\frac{\partial \rho'}{\partial t} + \rho_0 \nabla \cdot \vec{v}'_0 = 0 \tag{4.1.6}$$

which, for an isentropic fluid at constant entropy and with constant ambient density ρ_0

$$p' = c_0^2 \rho' \tag{4.1.7}$$

Where c_0 is the ambient speed of sound. Similarly, the linearized form of Eq. (4.1.1) can be written as

$$\rho_0 \, \frac{\partial \vec{v}'}{\partial t} = -\nabla p' \tag{4.1.8}$$

One can manipulate equations (4.1.4) - (4.1.6) in order to write a partial differential equation in terms of pressure (Crocker, 1998).

$$\nabla^2 p' + \frac{1}{c_0^2} \frac{\partial^2 \vec{p}}{\partial t^2} = 0 \tag{4.1.9}$$

Or in terms of acoustic velocity $\frac{\partial \vec{u}}{\partial t} = \vec{v}$,

$$\rho \frac{\partial^2 \vec{u}}{\partial t^2} - \nabla(\kappa_s \nabla \cdot \vec{u}) = 0 \tag{4.1.10}$$

where κ_s is bulk modulus defined as a product of the density and the speed of sound in the medium squared, $\kappa_s = \rho_0 c_0^2$.

Given that fluids do not withstand shear forces, the speed of sound would only change as a function of pressure and temperature.